



HAL
open science

TPLATE complex dependent endocytosis is required for shoot apical meristem maintenance by attenuating CLAVATA1 signaling

Jie Wang, Qihang Jiang, Roman Pleskot, Peter Grones, Grégoire Denay, Carlos Galván-Ampudia, Elmehdi Bahafid, Xiangyu Xu, Michael Vandorpe, Evelien Mylle, et al.

► To cite this version:

Jie Wang, Qihang Jiang, Roman Pleskot, Peter Grones, Grégoire Denay, et al.. TPLATE complex dependent endocytosis is required for shoot apical meristem maintenance by attenuating CLAVATA1 signaling. 2022. hal-03865506

HAL Id: hal-03865506

<https://cnrs.hal.science/hal-03865506v1>

Preprint submitted on 22 Nov 2022

HAL is a multi-disciplinary open access archive for the deposit and dissemination of scientific research documents, whether they are published or not. The documents may come from teaching and research institutions in France or abroad, or from public or private research centers.

L'archive ouverte pluridisciplinaire **HAL**, est destinée au dépôt et à la diffusion de documents scientifiques de niveau recherche, publiés ou non, émanant des établissements d'enseignement et de recherche français ou étrangers, des laboratoires publics ou privés.



Distributed under a Creative Commons Attribution - NonCommercial - NoDerivatives 4.0 International License

1 TPLATE complex dependent endocytosis is required for shoot apical meristem maintenance by
2 attenuating CLAVATA1 signaling

3 Jie Wang^{1,2}, Qihang Jiang^{1,2}, Roman Pleskot^{1,2,3}, Peter Grones^{1,2}, Grégoire Denay^{4,5},
4 Carlos Galván-Ampudia⁶, Elmehdi Bahafid^{4,5}, Xiangyu Xu^{1,2}, Michael Vandorpe^{1,2},
5 Evelien Mylle^{1,2}, Ive De Smet^{1,2}, Teva Vernoux⁶, Rüdiger Simon^{4,5}, Moritz K. Nowack^{1,2},
6 Daniel Van Damme^{1,2,*}

7 ¹Ghent University, Department of Plant Biotechnology and Bioinformatics,
8 Technologiepark 71, 9052 Ghent, Belgium

9 ²VIB Center for Plant Systems Biology, Technologiepark 71, 9052 Ghent, Belgium

10 ³Institute of Experimental Botany, Czech Academy of Sciences, 165 02 Prague, Czech
11 Republic

12 ⁴Institute for Developmental Genetics, Heinrich-Heine University, University Street 1, D-
13 40225 Düsseldorf, Germany

14 ⁵Cluster of Excellence on Plant Sciences (CEPLAS), University Street 1, D-40225
15 Düsseldorf, German

16 ⁶Laboratoire Reproduction et Développement des Plantes, Univ Lyon, ENS de Lyon,
17 CNRS, INRAE, France

18 *Correspondence: daniel.vandamme@psb.vib-ugent.be (D.V.D.)

19

20

21

22

23

24

25

26

27

28 **Abstract**

29 Endocytosis regulates the turnover of cell surface localized receptors, which are crucial
30 for plants to sense and rapidly respond to both endogenous and environmental stimuli.
31 The evolutionarily ancient TPLATE complex (TPC) plays an essential role in clathrin-
32 mediated endocytosis (CME) in Arabidopsis plants. Knockout or strong knockdown of
33 single TPC subunits causes male sterility and seedling lethality phenotypes, complicating
34 analysis of the roles of TPC during plant development. Partially functional alleles of TPC
35 subunits however only cause very mild developmental deviations. Here, we took
36 advantage of the recently reported partially functional TPLATE allele, WDXM2, to
37 investigate a role for TPC-dependent endocytosis in receptor-mediated signalling. We
38 discovered that reduced TPC-dependent endocytosis confers a hypersensitivity to very
39 low doses of CLAVATA3 (CLV3) peptide signalling. This hypersensitivity correlated with
40 the abundance of the CLV3 receptor protein kinase CLAVATA1 (CLV1) at the plasma
41 membrane. Genetic analysis and live-cell imaging revealed that TPC-dependent
42 regulation of CLV3-dependent internalization of CLV1 from the plasma membrane is
43 required for CLV3 function in the shoot. Our findings provide evidence that clathrin-
44 mediated endocytosis of CLV1 is a mechanism to dampen CLV3-mediated signaling
45 during plant development.

46

47 **Key Words:** Clathrin-mediated endocytosis, TPLATE complex, CLAVATA3-CLAVATA1
48 signaling, shoot apical meristem maintenance

49

50

51

52

53

54

55

56

57

58 Introduction

59 Coordinating cellular responses to environmental stimuli largely relies on receptor-like
60 kinases (RLKs) or receptor-like proteins (RLPs) localized on the plasma membrane (PM),
61 that are activated by cognate peptide ligands (Claus *et al*, 2018; Gou & Li, 2020;
62 Hohmann *et al*, 2017; Olsson *et al*, 2019). CLAVATA1 (CLV1)-type receptors are one of
63 the most intensively studied groups of plant RLKs, and they are crucial for shoot apical
64 meristem (SAM) and root apical meristem (RAM) maintenance (Clark *et al*, 1993; Clark
65 *et al*, 1997; DeYoung *et al*, 2006; Deyoung & Clark, 2008; Dievart *et al*, 2003; Stahl *et al*,
66 2013). PM abundance and vacuolar targeting of CLV1 depends on the CLAVATA3 (CLV3)
67 peptide (Nimchuk *et al*, 2011). However, how CLV1 signaling is modulated by its
68 internalization remains unknown (Yamaguchi *et al*, 2016).

69 In plants, clathrin-mediated endocytosis (CME) is the best-characterized pathway by
70 which cells internalize transporters, receptors and their bound ligands from PM via
71 transport vesicles (Paez Valencia *et al*, 2016; Zhang *et al*, 2015). Internalization of PM
72 localized receptors can occur in a ligand-independent or ligand-dependent manner (Beck
73 *et al*, 2012; Ben Khaled *et al*, 2015; Irani *et al*, 2012; Mbengue M, 2016; Nimchuk *et al*,
74 2011; Ortiz-Morea *et al*, 2016) and serves either to attenuate signalling by vacuolar
75 degradation or to sustain signalling from endosomes (Claus *et al*, 2018; Paez Valencia
76 *et al*, 2016).

77 The heterotetrameric adaptor protein complex 2 (AP-2) and the octameric TPLATE
78 complex (TPC) jointly function as adaptor complexes to execute CME in plants (Di Rubbo
79 *et al*, 2013; Gadeyne *et al*, 2014; Zhang *et al*, 2015). Knockout or strong knockdown of
80 single TPC subunits results in pollen and seedling lethality (Gadeyne *et al*, 2014; Van
81 Damme *et al*, 2006; Wang *et al*, 2019). Mild knockdown of TPC subunits or destabilization
82 of TPC by mutating the evolutionary most conserved domain (the WDX domain) in the
83 TPLATE subunit, however, results in viable plants, allowing to address possible
84 developmental functions for this complex (Bashline *et al*, 2015; Van Damme *et al*, 2006;
85 Wang *et al*, 2021).

86 In this study, we took advantage of WDX domain-dependent TPC destabilization to
87 explore how reduced TPC-dependent endocytic capacity affects receptor-mediated
88 signaling in plants. We compared the response of control plants (*tplate(-/-)*
89 complemented with TPLATE-GFP) with that of plants expressing the partially functional
90 allele (*tplate(-/-)* complemented with WDXM2-GFP) upon exposure to different types of
91 exogenous peptides.

92 **Results and discussion**

93 **Reduced TPC-dependent endocytosis confers hypersensitivity to a subset of CLE** 94 **peptides**

95 *In vitro* bioassays comparing root growth in the presence or absence of exogenous
96 peptide ligands provide an easy readout and are widely employed to evaluate how plants
97 respond to peptide-dependent signaling (Anne *et al*, 2018; Blumke *et al*, 2021; Breda *et*
98 *al*, 2019; Graeff *et al*, 2020; Hazak *et al*, 2017; Hu *et al*, 2018; Poncini *et al*, 2017). To
99 correlate peptide-dependent receptor signalling with CME capacity, we selected several
100 classes of peptide ligands. CME has been shown to internalize the pattern recognition
101 receptors PEP RECEPTOR1 (PEPR1) and FLAGELLIN SENSING 2 (FLS2), which are
102 the respective receptors of the *Arabidopsis thaliana* endogenous elicitor peptides
103 (AtPEPs) and the bacterial peptide FLAGELLIN 22 (FLG22) (Mbengue M, 2016; Ortiz-
104 Morea *et al.*, 2016). We also included the C-TERMINALLY ENCODED PEPTIDE 5
105 (CEP5), which impacts on primary root length and lateral root initiation via its proposed
106 receptor XYLEM INTERMIXED WITH PHLOEM 1 (XIP1)/CEP RECEPTOR 1 (CEPR1)
107 (Roberts *et al*, 2016). Finally, we included fourteen CLV3/EMBRYO SURROUNDING
108 REGION (CLE) peptides, which are essential for shoot and root meristem maintenance
109 by activating various plasma membrane-bound receptors (Yamaguchi *et al.*, 2016).

110 TPLATE and WDXM2 complemented seedlings were grown in the presence of
111 different CLE peptides. The majority of the tested CLE peptides, which were applied at
112 nanomolar concentrations, elicited a similar response in WDXM2 and TPLATE seedlings
113 (Fig EV1A-B). However, we observed a strong hypersensitivity of WDXM2 seedlings to
114 CLV3, CLE10 and CLE40 (Fig EV1A-B). CLE40 is the closest homolog of CLV3 in
115 *Arabidopsis*, and both peptides are crucial for root and shoot meristem maintenance
116 (Brand *et al*, 2000; Clark *et al*, 1995; Fletcher *et al*, 1999; Hobe *et al*, 2003; Ito *et al*, 2006;
117 Schlegel *et al*, 2021; Stahl *et al.*, 2013; Stahl *et al*, 2009; Yamaguchi *et al.*, 2016). The
118 specific hypersensitivity of the WDXM2 expressing seedlings to these two closely related
119 peptides hinted towards a connection between TPC-dependent endocytosis and CLV1-
120 type receptor signalling.

121 We subsequently treated TPLATE and WDXM2 complemented plants with CLV3, CLE40
122 at a concentration of 10 nM as well as with different doses of FLG22, AtPEP1 and CEP5
123 peptides, previously shown to affect root growth (Poncini *et al.*, 2017), and we compared
124 the effect between our two backgrounds that differ in their endocytic capacity (Wang *et*
125 *al.*, 2021). After a 5-day exposure, both WDXM2 and TPLATE seedlings, grown in the

126 presence of the peptides, showed reduced root growth compared to the control situation,
127 indicating that they responded to the treatments. In contrast to the clearly differential
128 effect observed for CLV3 and CLE40 (Fig 1A-B), both backgrounds responded similarly
129 to FLG22 treatment and only a slight but statistically significant difference was found in
130 response to the low dose of AtPEP1 but not to the higher dose (Fig 1C-D). We also did
131 not observe any differential response between TPLATE and WDXM2 complemented
132 plants to both low and high doses of CEP5, although the latter severely reduced root
133 growth (Fig 1C-D). These results indicate that the differential endocytic capacity between
134 both backgrounds elicits hypersensitivity to CLE peptides, but that the mild endocytic flux
135 difference between both backgrounds is insufficient to generate a differential
136 developmental effect due to FLG22-, AtPEP1- or CEP5-dependent receptor signaling at
137 the concentrations used. We conclude that regulatory mechanisms controlling the activity
138 of those receptors remain sufficiently active in both genetic backgrounds.

139 To independently confirm the observed hypersensitivity to CLV3 and CLE40, we tested
140 the *twd40-2-3* mutant. This is a mild knockdown allele of the TPC subunit TWD40-2
141 (Bashline *et al.*, 2015). Similar to our partially functional WDXM2 allele, *twd40-2-3* mutant
142 plants also exhibited a hypersensitive response to low doses of CLV3 and CLE40
143 treatment (Fig EV2). Altogether, these results revealed that reduced TPC-dependent
144 endocytosis enhances CLV3 and CLE40 signalling in Arabidopsis roots.

145 **TPC-dependent endocytosis contributes to SAM maintenance through the** 146 **WUSCHEL signalling pathway**

147 Next to root meristem maintenance, CLV3-dependent signaling is also essential to
148 maintain SAM homeostasis. Long-term synthetic CLV3 peptide treatment dampens cell
149 proliferation and thus consumes SAM (Hu *et al.*, 2018; Ishida *et al.*, 2014). To investigate
150 the importance of TPC-dependent endocytosis for SAM maintenance, we compared the
151 sensitivity of TPLATE and WDXM2 complemented plants to long-term CLV3 peptide
152 treatment. Seedling morphologies indicated that TPLATE and WDXM2 seedlings were
153 equally capable of maintaining their SAM in the presence of very low doses of exogenous
154 CLV3 peptides (10 nM), even during long-term treatment (Fig 2A-B). However, higher
155 concentrations (100 nM and 1 μ M) of CLV3 revealed hypersensitivity of WDXM2
156 seedlings and increasingly caused SAM termination in independent mutant WDXM2 lines
157 (Fig 2A-B and Fig EV3A-B). The hypersensitivity of WDXM2 plants to CLV3 further
158 correlated with the protein levels of the complementation constructs in the complemented
159 *tplate* mutant lines (Fig EV3C). These results suggest that TPC-dependent endocytic

160 deficiency causes a dose-dependent hypersensitivity to CLV3-dependent receptor
161 signalling.

162 In the SAM, CLV3 signalling functions in a negative feedback circuit to dampen stem
163 cell proliferation by regulating the expression of the homeodomain transcription factor
164 WUSCHEL (*WUS*) (Hazak & Hardtke, 2016; Kitagawa & Jackson, 2019; Yamaguchi *et*
165 *al.*, 2016). To further examine whether TPC-dependent endocytosis is involved in the
166 CLV–*WUS* feedback loop to regulate SAM homeostasis, we analyzed the expression
167 patterns of *WUS* in TPLATE and WDXM2 complemented plants following a three-day
168 CLV3 peptide treatment. Both 10 nM and 100 nM CLV3 peptide treatment did not visibly
169 impair *WUS* promoter activity in TPLATE vegetative SAMs at the seedling level compared
170 to control conditions as visualized by GUS staining (Fig 2C-D). In WDXM2 vegetative
171 SAMs, however, CLV3 application dampened *WUS* expression in a dose-dependent
172 manner (Fig 2C-D), which is coherent with the terminated SAM phenotype observed at
173 the rosette stage level upon prolonged treatment (Fig 2A-B). These findings reveal that
174 TPC-dependent endocytosis is involved in the regulation of CLV3-*WUS* signaling in the
175 SAM.

176 **TPC-dependent endocytosis internalizes CLV1 to dampen CLV3-dependent** 177 **signalling**

178 The receptor kinase CLV1 signals in response to CLV3 and plays a central role in shoot
179 meristem maintenance (Brand *et al.*, 2000; Clark *et al.*, 1997; Fletcher *et al.*, 1999;
180 Ogawa *et al.*, 2008; Shinohara & Matsubayashi, 2015; Somssich *et al.*, 2015). CLV1 levels
181 increase at PM in the absence of CLV3 and accumulate in the vacuole in the presence
182 of CLV3 (Nimchuk *et al.*, 2011). CLV3-induced vacuolar accumulation of CLV1 suggests
183 a negative regulation of CLV3/CLV1 signaling by internalization, yet this hypothesis
184 remains to be experimentally tested (Yamaguchi *et al.*, 2016).

185 To characterize whether TPC-dependent endocytosis functions in CLV1 internalization,
186 we evaluated whether the response of TPLATE and WDXM2 complemented plants to
187 CLV3 treatment depended on the presence of CLV1. Combining the *clv1-101* null allele
188 (Atsuko Kinoshita, 2010) with our TPLATE and WDXM2 complemented plants largely
189 suppressed the hypersensitivity to exogenous CLV3 leading to SAM termination in
190 WDXM2, although not completely (Fig 3A-B). Combining the strong and dominant-
191 negative *clv1* mutant allele *clv1-8* (Clark *et al.*, 1997; Dievart *et al.*, 2003) restored SAM
192 maintenance in WDXM2 in the presence of 100nM CLV3 (Fig 3A-B). The differential
193 effect of exogenous CLV3 on SAM activity between WDXM2, WDXM2/*clv1-101* and

194 WDXM2/*clv1-8* was also apparent in the number of leaves that the plants produced (Fig
195 3C).

196 These results reveal that CLV1 predominantly contributes to the hypersensitivity of
197 CLV3-dependent signalling in WDXM2 mutant plants. The different capacity of the *clv1-101*
198 null allele and the *clv1-8* dominant negative allele to reduce the sensitivity of WDXM2
199 to CLV3 is likely attributed to genetic redundancy within the CLV1 receptor family
200 (DeYoung *et al.*, 2006; Deyoung & Clark, 2008; Nimchuk, 2017; Nimchuk *et al.*, 2015;
201 Shinohara & Matsubayashi, 2015).

202 The WDXM mutation destabilizes TPC and thereby negatively affects endocytic
203 capacity (Wang *et al.*, 2021). The entire TPC complex is required to execute CME at PM
204 (Gadeyne *et al.*, 2014; Johnson *et al.*, 2021; Wang *et al.*, 2020; Wang *et al.*, 2021;
205 Yperman *et al.*, 2021b) and destabilizing TPC in WDXM2 complemented plants impairs
206 endocytic capacity while it does not affect recruitment of the two AtEH/Pan1 subunits at
207 PM, which are involved in promoting autophagy (Wang *et al.*, 2021; Wang *et al.*, 2019).
208 It is therefore likely that the CLV1-dependent hypersensitivity to CLV3 is linked to altered
209 endocytosis of CLV1 in WDXM2. CLV1 is a master regulator of flower development (Clark
210 *et al.*, 1997; Schoof *et al.*, 2000). Both TPLATE and WDXM2 are expressed in the
211 inflorescence meristem at roughly similar levels although in these tissues, WDXM2
212 appears to be slightly less PM-associated compared to TPLATE (Fig EV4A). Next, we
213 monitored the PM localization of functional CLV1-GFP in the inflorescence meristems of
214 TPLATE and WDXM2 plants. We observed similar levels of CLV1-GFP on the PM in
215 WDXM2 inflorescence meristems compared with TPLATE plants (Fig EV4). In vegetative
216 meristems, however, our live imaging analysis clearly showed increased levels of CLV1-
217 GFP in the WDXM2 background (Fig 4A).

218 CLV1 undergoes CLV3-mediated degradation in inflorescence meristems upon
219 induction of *CLV3* expression in the *clv3-2* mutant background (Nimchuk *et al.*, 2011). In
220 vegetative meristems and in the presence of endogenous levels of CLV3, signal
221 intensities of CLV1 showed variation before and after exogenous CLV3 application. Live
222 cell imaging of the same vegetative meristem before and after CLV3 addition (Fig EV5A)
223 as well as quantification of treated and untreated meristems however revealed that CLV1
224 levels significantly reduced upon long-term (present in the medium from germination
225 onward; Fig 4) or short-term (10 and 30min; Fig EV5B-E) exogenous CLV3 application
226 in TPLATE seedlings, while this was not the case in WDXM2 seedlings (Fig 4; Fig EV5B-
227 E).

228 These results strongly correlate the endocytosis deficiency in WDXM2 with impaired
229 internalization of CLV1 in vegetative meristems. Increased CLV1 levels at PM are also in
230 accordance with the fact that WDXM2 complemented plants are hypersensitive to CLV3
231 peptide treatment, which correlates with strongly reduced *WUS* levels and therefore likely
232 increased CLV1-mediated transcriptional repression (Fig 2 and Fig 3). Despite this
233 hypersensitivity, vegetative SAMs in WDXM2 appear enlarged compared to those in
234 TPLATE control seedlings (Fig 4 and Fig EV5). How this relates to the abundance of
235 CLV1 at PM and to altered *WUS* levels remains to be determined.

236 To establish a direct link between CLV1 and TPC, we examined the interaction
237 between TPC and CLV1. TPC, visualized using an antibody against TPLATE, specifically
238 co-purified with CLV1 in Arabidopsis seedlings when CLV1-2xGFP was used as bait (Fig
239 5A). Next, we aimed to confirm this interaction and to determine which adaptor complex
240 subunits were involved. Tyrosine motif-based cargo recognition involves the medium
241 subunit of the Adaptor protein 2 complex, AP-2M (Arora & Damme, 2021), whose
242 counterpart in TPC is the TML subunit. Furthermore, TPLATE co-purified with CLV1 (Fig
243 5A) and AtEH1/Pan1 was shown to interact with cargo (Yperman *et al.*, 2021a). We
244 therefore selected these proteins for ratiometric bimolecular fluorescence
245 complementation (rBiFC) in *N. benthamiana*. Similar to previous experiments, the
246 shaggy-like kinase BIN2 served as negative control (Arora *et al.*, 2020). We could not
247 visualize interaction between CLV1 and TPLATE, TML or AP-2M in this system (Fig 5B-
248 C). Our confocal analysis, however, clearly linked CLV1 to the plant-specific TPC subunit
249 AtEH1/Pan1 (Gadeyne *et al.*, 2014; Hirst *et al.*, 2014) in the presence and absence of
250 exogenous CLV3 peptide (Fig 5B-C). The interaction between CLV1 and AtEH1/Pan1
251 was further assessed via yeast-two-hybrid (Y2H) using the cytoplasmic part of CLV1 and
252 the N-terminal part of AtEH1/Pan1 ending just after the second EH domain (Yperman *et al.*,
253 2021b). In total, 24 independent double transformations, combining CLV1 with
254 AtEH1/Pan1, CLV1 with empty vector control or AtEH1/Pan1 with empty vector control
255 were compared, alongside 8 double transformations of the empty vector control and the
256 p53-SV40 positive control (Fig 5D). The results clearly show a specific interaction
257 between CLV1 and AtEH1/Pan1 (Fig 5D). Both rBiFC and Y2H therefore clearly link the
258 cytoplasmic part of CLV1 to the N-terminal part of AtEH1/Pan1. The N-terminal located
259 EH domains of AtEH1/Pan1 were previously also shown to be involved in membrane
260 recruitment of TPC as well as in the internalization of the Secretory Carrier Membrane
261 Protein 5 (SCAMP5) via its double NPF motif (Johnson *et al.*, 2021; Yperman *et al.*,
262 2021a). CLV1, in contrast to SCAMP5, does however not contain obvious NPF motifs.

263 How CLV1 is recognized by AtEH1/Pan1 therefore remains to be determined.

264 Taken together, our findings reveal that the hypersensitivity of WDXM2 complemented
265 plants to CLV3 is most likely a consequence of sustained signalling from the PM in
266 vegetative meristems, which is caused by impaired internalization of CLV1 due to
267 reduced TPC-dependent endocytosis. TPC-dependent endocytosis, therefore, serves to
268 internalize CLV1 to attenuate CLV3 signalling to prevent meristem termination. Our work
269 thus identifies CME as a mechanism to control the availability of CLV1 at the PM and to
270 tune the activity of the shoot stem cell niche during plant development.

271 **Materials and Methods**

272 ***Molecular cloning***

273 mSCARLET (Bindels *et al*, 2017) was amplified with a stop codon from plasmid pEB2-
274 mSCARLET (Addgene,104006), introduced into pDONRP2R-P3 via a Gateway BP
275 reaction (Invitrogen) and confirmed by sequencing. To generate mSCARLET-fused
276 expression constructs of TPLATE and WDXM2, The pDONR221-TPLATE and
277 pDONR221-WDXM2 motif substituted entry clones (Wang *et al.*, 2021) were combined
278 with pHm34GW (Karimi *et al*, 2007), pDONRP4-P1r-Lat52 (Van Damme *et al.*, 2006),
279 and pDONRP2R-P3-mSCARLET in triple gateway LR reactions (Invitrogen).

280 The pBiFCt-2in1 BiFC vectors, which allow quantification of the observed Bimolecular
281 YPF fluorescence complementation by measuring the ratio between the intensity of the
282 YPF signal for a specific pair of interacting proteins and the intensity of the constitutively
283 expressed RFP which is present on the backbone of the vector, were used to generate
284 CLV1 related rBiFC constructs (Grefen & Blatt, 2012). The CLV1 entry clone for rBiFC
285 reactions was amplified from a published plasmid (Schlegel *et al.*, 2021), while TPLATE,
286 TML, AtEH1/Pan1 and AP2M were obtained from previously reported rBiFC experiments
287 (Arora *et al.*, 2020; Liu *et al*, 2020; Yperman *et al.*, 2021a). Entry clones were assembled
288 in an empty rBiFC destination vector (pBiFCt-2in1-CC, Addgene 105114 or pBiFCt-2in1-
289 NC, Addgene 105112) with a Gateway LR recombination reaction and selected using LB
290 containing spectinomycin and Xgall. The final rBiFC vectors were checked by restriction
291 digestion and sequencing of the recombination borders. For Y2H, the N-terminal domain
292 of AtEH1/Pan1 (AA 1-527) was amplified using following primer pairs (AtEH1_1-
293 527_GBD_F GCCATGGAGGCCGAATTCCTCAATGGCGGGTCAGAATCCTAACATGG
294 and AtEH1_1-527_GBD_R CTGCAGGTTCGACGGATCCCCTTATGCAGAATATCCATT
295 ACCTAGGTGATTAGC) and cloned into the pGBKT7 vector (Clontech). The cytoplasmic

296 part of CLV1 (AA 671 to 980, corresponding to the end of the transmembrane helix, from
297 amino acids LAWKL to the end of the uniprot sequence Q9SYQ8) was amplified using
298 following primer pairs (CLV1_671-980_GAD_F GAGGCCAGTGAATTCCACCCACTCG
299 CCTGGAAACTAACCGCCTTC and CLV1_671-980_GAD_R TCCCGTATCGATGCCC
300 ACCCTTAGAACGCGATCAAGTTCGCCACGG) and cloned into pGADT7 (Clontech).
301 Both vectors were generated via Gibson assembly following Smal-dependent
302 linearization of the vectors. Plasmids were verified using sequencing.

303 ***Arabidopsis transgenic lines and growth conditions***

304 All plant materials used in this research are in the Columbia-0 (Col-0) ecotype
305 background. Information on plant materials is listed in Table EV1. To generate the
306 mSCARLET fusions of transgenic lines, *tplate* heterozygous mutant plants were identified
307 by genotyping PCR and were transformed with expression constructs of TPLATE and
308 WDXM2 fused to mSCARLET under the control of LAT52 promoter as described before
309 (Van Damme *et al.*, 2006; Wang *et al.*, 2021; Yperman *et al.*, 2021b). Primary
310 transformants were selected with Hygromycin, and those carrying the *tplate* T-DNA
311 insertion were identified via genotyping PCR. The complemented lines in the T2
312 generation were further genotyped to identify homozygous *tplate* mutants (Wang *et al.*,
313 2021).

314 For all the crosses, the same reporter line or mutant plant was used as male to cross with
315 TPLATE and WDXM2 complemented lines respectively. The *pWUS::GUS* (Su *et al.*, 2009)
316 reporter line was crossed into TPLATE_1 and WDXM2_1 complemented mutant
317 backgrounds. In the progeny, F2 plants were genotyped to obtain homozygous *tplate*
318 mutant backgrounds. The F3 or F4 generation plants were screened to identify
319 homozygous plants for *pWUS::GUS* expression by GUS staining. The *clv1* null mutant
320 *clv1-101* (Atsuko Kinoshita, 2010) and the dominant-negative *clv1-8* mutant (Dievart *et*
321 *al.*, 2003) were crossed into the TPLATE_1 and WDXM2_1 complemented lines. The F2
322 or F3 generation plants were genotyped or sequenced to identify the *tplate/clv1-101* or
323 *tplate/clv1-8* double mutant backgrounds. To introduce the CLV1 marker line into
324 TPLATE and WDXM2 complemented lines, a wild type Col-0 plant expressing the
325 functional pCLV1::CLV1-GFP (Schlegel *et al.*, 2021) was backcrossed to Col-0 and a
326 single locus expression F2 line was identified by segregation using Basta (20 mg/L)
327 selection. Then the F2 Basta resistant CLV1-GFP expressing plant was used to cross
328 with the TPLATE_3 and WDXM2_3 complemented plants. In the progeny, plants
329 homozygous for the *tplate* mutant background were identified by genotyping PCR while

330 homozygous expression of CLV1-GFP was selected by segregation on BASTA. For co-
331 IP experiments, the pCLV1::CLV1-2xGFP line was used (Nimchuk *et al.*, 2011).

332 Seeds were sterilized by chlorine gas sterilization and sown on ½ MS medium plates
333 without sugar following a 3-day vernalization period at 4°C. Seedlings were grown in a
334 growth chamber under continuous light conditions at 21°C.

335 ***Phenotypic analysis***

336 Sequences of CLE peptides described before (Yamaguchi *et al.*, 2016) were ordered
337 from GeneScript. Information on the peptides is listed in Table EV2. For shoot treatments,
338 seedlings were grown horizontally on ½ MS medium supplemented with or without the
339 indicated concentration of CLV3 peptide for 3 weeks. Plants with terminated shoots were
340 counted manually. For root growth assays, seedlings were initially grown on ½ MS
341 medium supplemented with or without CLE peptides for a certain duration (data depicted
342 in Figure EV1). For the FLG22, AtPEP, CEB5, CLV3 and CLE40 peptides depicted in
343 Figure 1 and in Figure 2, seedlings were grown on ½ MS plates and then transferred to
344 plates with and without the indicated amount of peptides. Plates with seedlings were
345 scanned and root lengths were measured with the Fiji software package
346 (<https://imagej.net/software/fiji/>) equipped with the NeuronJ plugin (Meijering *et al.*, 2004).
347 Quantification of the number of leaves in Figure 3C was done manually using the cell
348 counter plugin in Fiji.

349 ***GUS staining***

350 GUS staining was performed as described before (Lammens *et al.*, 2008). Seedlings (3-
351 days after putting the plates in continuous light, i.e. roughly one day after germination)
352 expressing *pWUS::GUS* grown on ½ MS with or without CLV3 peptide were harvested
353 and incubated with 80% cold acetone for 30 min. After that, seedlings were washed with
354 phosphate buffer (pH = 7.2), incubated in GUS staining solution (1 mg/ml of 5-bromo-4-
355 chromo-3-indolyl β-D-glucuronide, 2 mM ferricyanide, and 0.5 mM ferrocyanide in 100
356 mM phosphate buffer pH 7.2) and kept at 37 °C in the dark for 3 hours. After GUS staining,
357 seedlings were cleared with lactic acid and visualized between slide and coverslip on a
358 BX51 light microscope (Olympus) using a 10x or 20x magnification.

359 ***Nicotiana benthamiana infiltration***

360 Three- to four-week-old *Nicotiana benthamiana* plants grown in greenhouse under long-

361 day conditions (06-22 h light, 100 PAR, 21° C) were used for infiltration as described
362 before (Arora *et al.*, 2020). 3 days after infiltration, *N. benthamiana* leaves were imaged
363 with an SP8X confocal microscope. CLV3 peptide (1 µM) in infiltration buffer (10 mM
364 MgCl₂ and 10 mM MES, pH 5.6) was applied via leaf infiltration. After 5 min incubation,
365 the injected samples were imaged within 30 min.

366 **Live-Cell Imaging and Analysis**

367 A Leica SP8X confocal microscope equipped with a white laser was used for all confocal
368 imaging via a 40x (HC PL APO CS2, NA=1.10) water- immersion corrected objective
369 except the flower meristem imaging.

370 rBiFC images were acquired with Hybrid detectors (HyDTM) using a time-gated window
371 between 0.3 ns-6.0 ns and in line sequential mode. YFP signals were acquired using
372 WLL 514 nm excitation and an emission window of 520-550 nm, and RFP signals were
373 detected using WLL 561 nm excitation and an emission window of 580-650 nm. All
374 images were taken using the same settings for YFP and RFP detection and saturation
375 was avoided in order not to interfere with the ratiometric quantification.

376 For CLV1-GFP imaging in vegetative SAMs in Figure 4 and Figure EV5B-E, seeds
377 expressing CLV1-GFP in TPLATE and WDXM2 complemented mutant backgrounds
378 were germinated on ½ MS plates supplemented with or without 100 nM of CLV3 peptide.
379 Seedlings were imaged following 3-days after putting the plates in continuous light, which
380 roughly equals 1 day after germination. For CLV1-GFP imaging upon short-term CLV3
381 peptide treatment in Figure EV5, seedlings grown on ½ MS plates (3 days in light) were
382 used. After removal of the cotyledons, seedlings were incubated in ½ MS medium
383 containing 1 µM CLV3 peptide and 0.1% Tween 20 (v/v) for 10 or 30 min, and washed
384 with water shortly 3 times. Prior to imaging, seedlings expressing CLV1-GFP were
385 stained with PI solution (10 µg/mL) for 1 to 2 min. The Hybrid detectors (HyDTM) were
386 employed to image PI (excitation at 561 nm, emission between 600-700 nm) and CLV1-
387 GFP (excitation at 488 nm, emission between 500-540 nm) without (PI) or with (GFP) a
388 time-gated window between 0.3 ns-6.0 ns. To achieve sufficient signal when imaging
389 CLV1-GFP in the vegetative SAMs of TPLATE-3 and WDXM2_3 seedlings, accumulative
390 imaging was used. Images were acquired using 8 times line accumulation and 2 times
391 frame averaging.

392 For the flower SAM imaging in Figure EV4A, Arabidopsis plants were grown in soil for 4
393 weeks at 21 °C under long day condition (16 h light : 8 h dark, LED 150 µmol/m²/s).

394 Primary inflorescence shoot apical meristems were dissected, mounted in ACM and then
395 stained with 100 μ M propidium iodide (PI; Merck) for 5 min prior to imaging (Brunoud *et*
396 *al*, 2020). Meristems were imaged with a Zeiss LSM 710 spectral microscope using the
397 following settings: GFP (excitation at 488 nm, emission between 510-558 nm) and
398 propidium iodide (excitation 488 nm, emission between 605-650 nm).

399 For the flower SAM imaging in Figure EV4B, SAMs were imaged using a Zeiss LSM 780
400 confocal microscope (40 \times water immersion objective, Zeiss C-PlanApo, NA 1.2). Shoot
401 meristems were manually dissected by cutting of the stem, removing the flowers, and
402 were stained with 1 mg/ml DAPI. GFP was excited with an argon laser at 488 nm and
403 emission was detected between 490-530 nm, and mSCARLET was excited with Diode-
404 pumped solid state (DPSS) lasers at 514 nm and detected between 570-650 nm. DAPI
405 was excited at 405 nm with a laser diode and detected between 410-480 nm.

406

407 For CLV1-GFP imaging in vegetative SAMs in Figure EV5A, vegetative shoot apices at
408 3 DAG were manually dissected under a stereo microscope by removing the leaf
409 primordia. The cell wall was stained with PI. After removal of the leaf primordia, vegetative
410 SAMs were treated with $\frac{1}{2}$ MS medium containing 1 μ M CLV3 peptide and 0.1% Tween
411 20 and imaged at 0 min and 30 min after treatment. Z-stacks of vegetative SAMs were
412 acquired using a Zeiss LSM 780 confocal microscope (40 \times water immersion objective,
413 Zeiss C-PlanApo, NA 1.2). GFP was excited with an Argon laser at 488 nm and emission
414 was detected using a 490-530 nm window. PI was excited at 561 nm by a DPSS laser
415 and detected using a 590-650 nm window.

416 The quantification of rBiFC and SAM images was performed using Fiji. For rBiFC, a
417 region of interest (ROI) on PM of the cells was selected and the intensities of YFP and
418 RFP signals were measured. The ratios between YFP and RFP signals per cell were
419 then calculated and plotted. For the quantification of CLV1-GFP in TPLATE and WDXM2
420 vegetative SAMs, a region of interest (ROI) covering the meristem was defined and the
421 CLV1-GFP signal intensities were measured. Only images with less than 1% saturated
422 pixels were quantified. The histogram function in Fiji was used to generate intensity
423 values (8-bit gray values) for each pixel and the top 10% highest intensity pixels were
424 used to calculate the mean fluorescence intensities using an in-house designed script in
425 Microsoft Excel. Using a selection of the strongest intensity pixels for the calculations
426 omits background noise that otherwise reduces the average fluorescence intensities of
427 the quantifications and follows from the rationale that the fluorescence is linked to the
428 endomembrane system and therefore not continuously present throughout the selected

429 ROI. Similar approaches are also used to calculate ratios of endocytic flux between PM
430 and endosomal compartments (Dejonghe *et al*, 2016; Mishev *et al*, 2018).

431 ***Protein extraction and Western blotting***

432

433 Arabidopsis seedlings were grown for 5 days on ½ MS medium without sugar under
434 continuous light conditions. Seedlings were harvested, flash-frozen, and grinded in liquid
435 nitrogen. Proteins were extracted in a 1:1 ratio, buffer (ml):seedlings (g), in HB+ buffer,
436 as described before (Van Leene *et al*, 2015). Protein extracts were incubated for 30 min
437 at 4°C on a rotating wheel before spinning down twice at 20,000 g for 20 min. The
438 supernatant concentration was measured using the Bradford Protein Assay (Invitrogen),
439 and equal amounts of proteins were loaded on 4 to 20% gradient gels (Bio-Rad). Gels
440 were transferred to nitrocellulose membranes using the Trans-Blot Turbo system (Bio-
441 Rad). Blots were incubated with α-TPLATE appendage antibodies (rabbit) (Dejonghe *et*
442 *al*, 2019) and imaged on a ChemiDoc Imaging System (Bio-Rad).

443

444 **Co-immunoprecipitation**

445

446 Finely ground material was suspended in homogenization extraction buffer [150 mM Tris-
447 HCl, 150 mM NaCl, 0.5 mM EDTA, 10% glycerol, 1 mM sodium molybdate, 1 mM NaF,
448 10 mM DTT, 1% IGEPAL CA-630 (Sigma-Aldrich,USA) with Complete Ultra EDTA-free
449 Protease Inhibitor Cocktail Tablets (Roche, Switzerland; 1 tablet per 10 mL)]. After 30
450 min of rotation at 4 °C, cell debris was removed from the samples by centrifugation for
451 15 min at 2000 g at 4 °C. Supernatant was transferred to a new tube through Miracloth
452 (Millipore Sigma, USA). Then, 50 µL pre-equilibrated GFP-Trap®_MA beads
453 (ChromoTek, Germany) was added into each sample and samples were incubated for
454 2 h at 4 °C to maximize the protein binding. Afterwards, the beads were washed two times
455 with wash buffer (20 mM Tris-HCl pH 7.5, 150 mM NaCl). Protein was eluted from the
456 beads by adding Laemmli sample buffer (Bio-rad, Laboratories, Inc., USA), Sample
457 Reducing Agent (Invitrogen, USA) and incubating at 70 °C for 10 min.

458

459 The proteins were separated on 4–15% SDS-PAGE stain-free protein gel (Bio-Rad
460 Laboratories, Inc., USA), followed by transferring onto a Trans-Blot® Turbo™ Mini PVDF
461 Transfer Packs (Bio-Rad Laboratories, Inc., USA). After blocking with 5% Skim Milk
462 (Difco,USA) for 1 h at room temperature, blots were incubated with α GFP-HRP
463 (ChromoTek, Germany) (1:2000) or α TPLATE2 (rabbit) (Dejonghe *et al.*, 2019) overnight

464 at 4 °C. Imaging was done using Chemiluminescent substrate (Thermo Fisher Scientific,
465 USA) and detected by ChemiDoc™ MP Imaging System (Bio-Rad Laboratories, Inc.,
466 USA).

467

468 **Yeast two hybrid analysis**

469

470 The N-terminal part of AtEH1/Pan1 (AA 1-527) up to the coiled coil domain in pGBKT7
471 and the cytoplasmic part of CLV1 (AA 671-980) in pGADT7 were combined with each
472 other and with empty control plasmids using the Matchmaker™ Gold Yeast Two-Hybrid
473 System (Clontech). The vectors were co-transformed into the Y2Hgold MATa Yeast
474 strain. Auto-activation was tested by co-transforming each vector with the corresponding
475 empty pGADT7 and pGBKT7 vectors. The empty pGADT7 and pGBKT7 were also co-
476 transformed as a negative control and as a positive control, we used the pGADT7-SV40
477 T-Ag and pGBKT7-p53 supplied with the Matchmaker system (Clontech).

478 Colonies of double transformed yeasts were first selected on SD -Leu -Trp plates. After
479 3 days at 30 °C, colonies were picked and grown for 3 days in liquid -Leu -Trp medium
480 at 30 °C 200 rpm. Fully grown cultures were diluted 1/5 in -L-T-H and 10 µl was spotted
481 on SD -Leu -Trp and SD -Leu -Trp -His plates. Pictures were taken after 3 days at 30 °C.

482

483 **Statistical analysis**

484 The R package in R studio (www.rstudio.com) was used. Data were tested for normality
485 and heteroscedasticity, after which the multcomp package was used (Herberich *et al*,
486 2010).

487

488

489

490

491

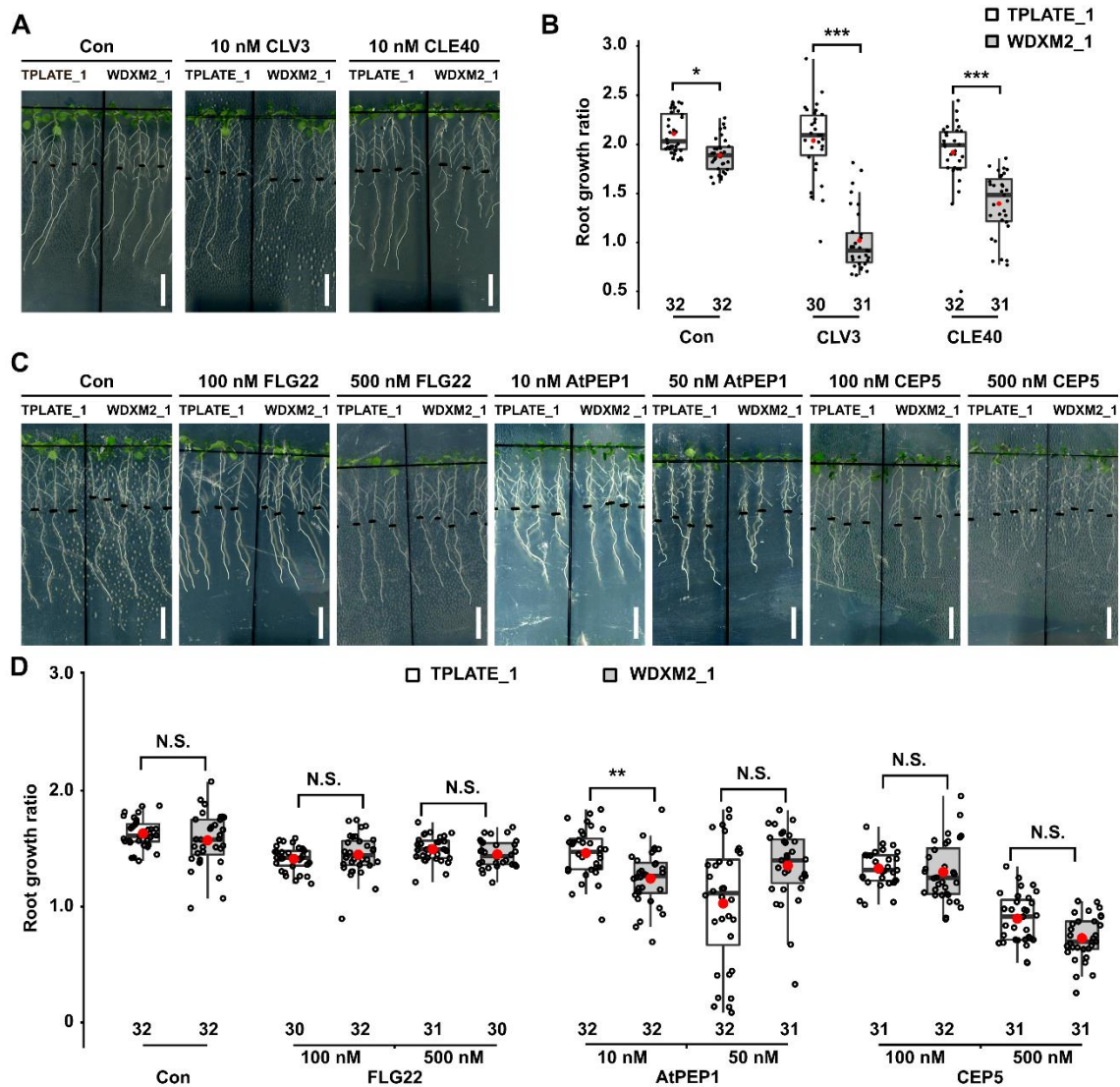
492

493

494

495

496 **Figures**

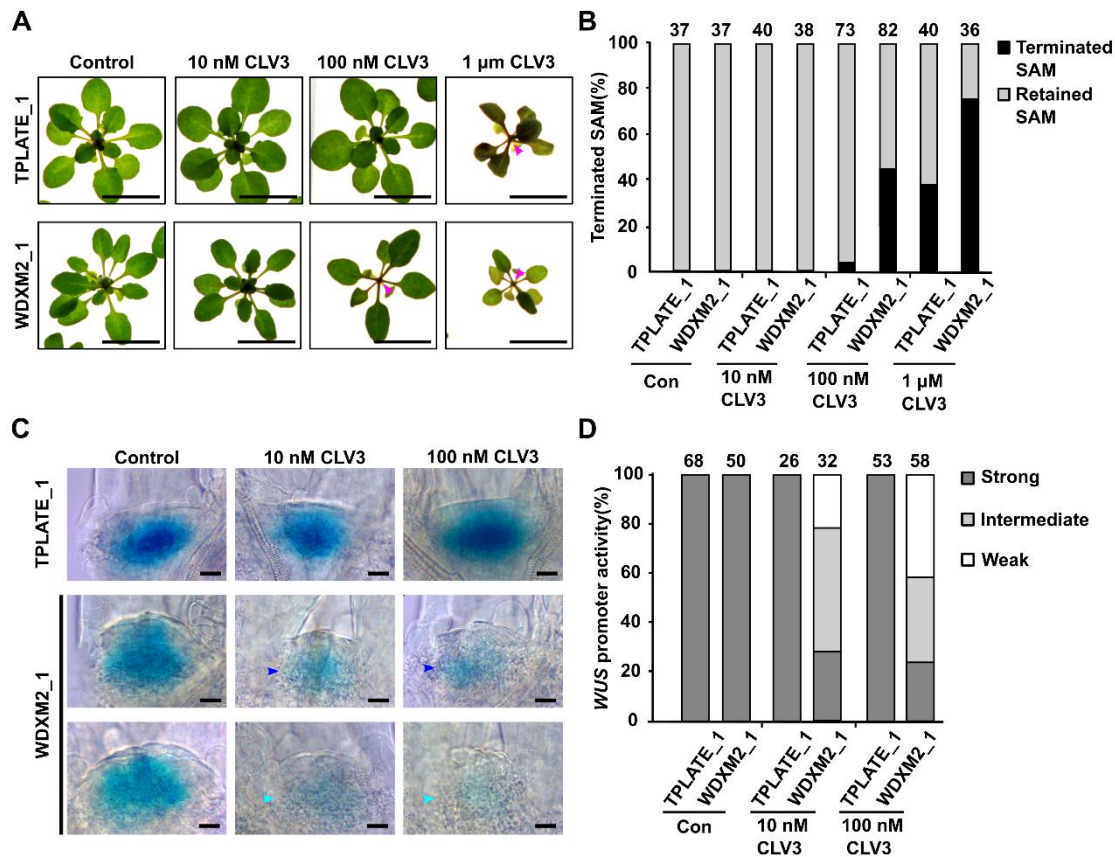


497

498 **Figure 1. Impaired TPC-dependent endocytic capacity confers hypersensitivity to CLV3 and CLE40**
 499 **peptides.**

500 (A-B) Representative images and quantification of the root growth ratios of TPLATE_1 and WDXM2_1
 501 seedlings (see Table EV1 for the specifications of the lines) treated with or without (Con) low doses of CLV3
 502 or CLE40 peptides. Scale bar = 1 cm. (C-D) Representative images and quantification of the root growth
 503 ratios of TPLATE_1 and WDXM2_1 seedlings treated with or without (Con) different doses of FLG22, CEP5
 504 and AtPEP1 peptides. 5-day-old seedlings grown vertically on ½ MS medium plate were transferred to freshly
 505 prepared ½ MS medium plates supplemented with or without low doses of peptides and grown vertically for
 506 an extra 5 days. For each individual root, the primary root length after the transfer was divided by the
 507 root length of the seedling before the transfer. The numbers at the bottom of the box plot and jitter box graphs
 508 represent the number of individual roots measured. The box plot extends from the 25th to 75th percentiles.
 509 The line inside the box marks the median. The whiskers go down and up to the 95% percentile. Data
 510 information in panel (B) and (D): Differences as compared to TPLATE complemented lines are indicated
 511 (selected pairs from Welch's ANOVA post hoc pairwise comparison with the Tukey contrasts); N.S., no

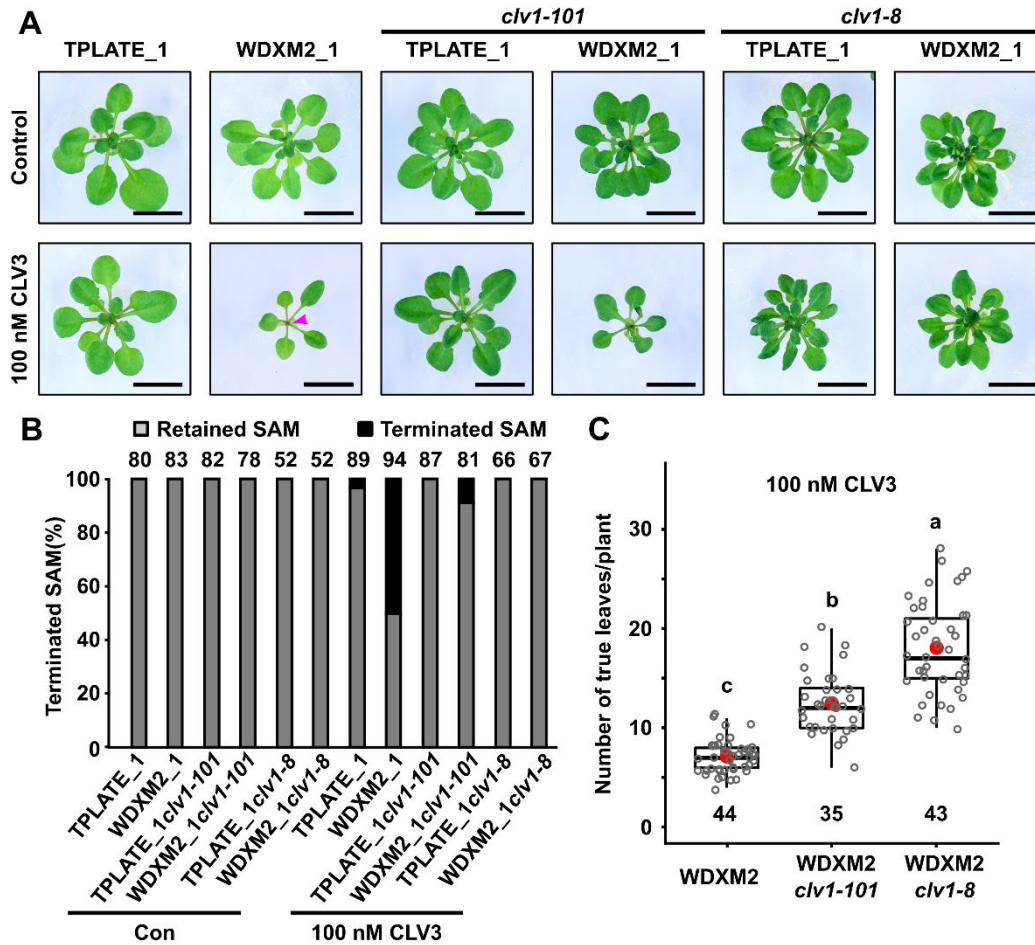
512 significant difference; *P < 0.05; **P < 0.01; ***P < 0.001. The data represented results from at least 4 sets
 513 of seedlings grown on separate plates.



514

515 **Figure 2. Impaired TPC-dependent endocytic capacity confers hypersensitivity to CLV3 in SAM.**

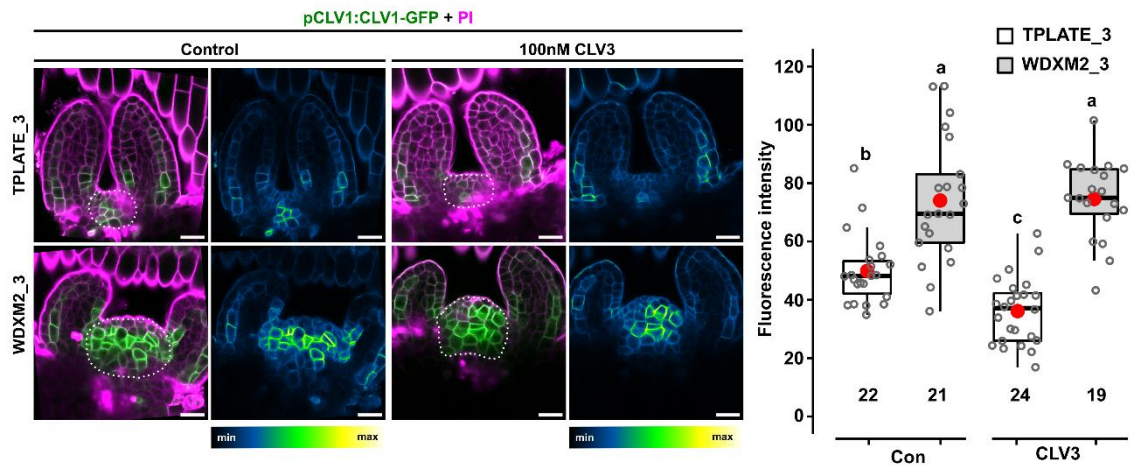
516 (A) Phenotypic comparison of 3- to 4-week-old TPLATE_1 and WDXM2_1 rosette stage plants grown on ½
 517 MS with or without different doses of CLV3 peptide. Magenta arrows indicate terminated SAMs. Scale bar =
 518 1cm. (B) Quantification of the amount of terminated shoot apical meristems in relation to the dose of CLV3
 519 applied. The number of plants used for the quantification is indicated at the top of the bar chart. (C-D)
 520 Representative images (C) and quantification (D) of *WUS::GUS* expression in the vegetative SAMs of 3-day-
 521 old TPLATE_1 and WDXM2_1 seedlings treated with or without different doses of CLV3 peptide.
 522 Intermediate (blue arrowhead) and weak (cyan arrowhead) *WUS* expression is indicated in the SAMs of
 523 WDXM2_1 seedlings after CLV3 treatment. Scale bar = 50 μm. *WUS* expression after CLV3 treatment was
 524 visually scored and quantified. The numbers of seedlings analyzed is indicated at the top of the bar chart.
 525 The data represented in panel A results from at least 5 sets of seedlings grown on separate plates. The data
 526 represented in panel D is the combination of two independent repetitions.



527

528 **Figure 3. CLV1 loss-of-function dampens CLV3 hypersensitivity in the SAMs of WDXM2**
 529 **complemented plants.**

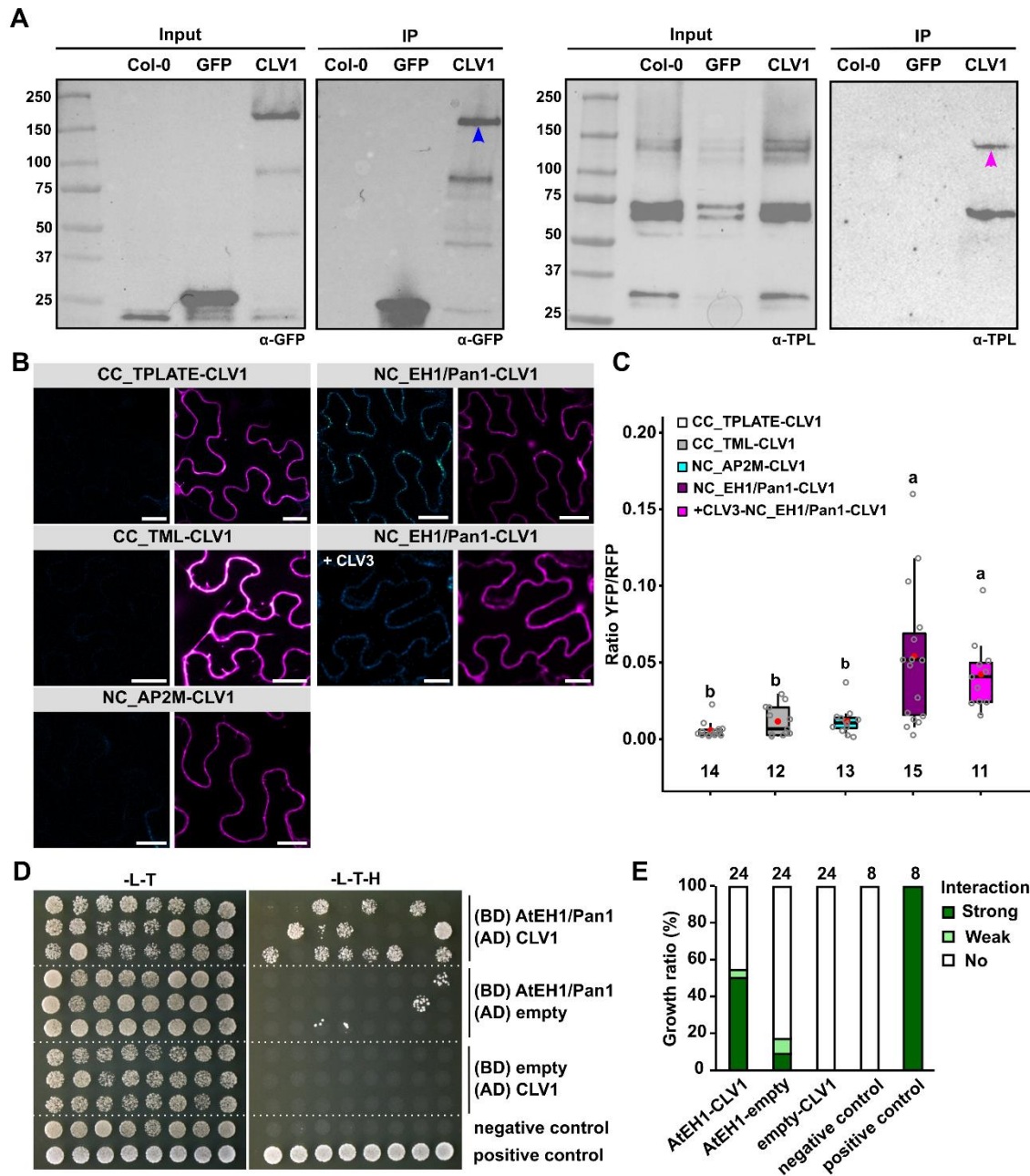
530 (A) Phenotypic comparisons of 3 to 4 -week-old TPLATE_1 and WDXM2_1 plants as well as combinations
 531 of these with the *clv1* null (*clv1-101*) or dominant negative (*clv1-8*) mutant backgrounds under control
 532 conditions or in the presence of 100 nM exogenous CLV3 peptide. The magenta arrowhead indicates a
 533 terminated SAM. Scale bar = 1 cm. (B) Quantification of the amount of terminated meristems in relation to the
 534 dose of CLV3 peptide applied. Numbers of plants used for quantification are indicated at the top of the bar
 535 chart. (C) Box plot and jitter box representation of the quantification of the number of leaves produced by
 536 WDXM2, WDXM2/*clv1-101* and WDXM2/*clv1-8* plants grown *in vitro* on medium supplemented with 100nM
 537 CLV3. Numbers of biological samples are indicated at the bottom of the box plot and jitter box graphs. The
 538 box plot extends from the 25th to 75th percentiles. The line inside the box marks the median. The whiskers
 539 go down and up to the 95% percentile. Letters (a, b and c) represent significantly different groups ($P < 0.001$)
 540 evaluated by Welch's ANOVA post hoc pairwise comparison with the Tukey contrasts. The data represented
 541 in panel B results from at least 6 sets of seedlings grown on separate plates. The data in panel C is based
 542 on a random selection of 3 to 4 plates from panel B.



543

544 **Figure 4. Reduced TPC-dependent endocytic capacity impairs internalization of CLV1 from the PM in**
545 **SAM cells.**

546 Confocal images and quantification of Arabidopsis seedlings showing enhanced PM localization of CLV1-
547 GFP in WDXM2_3 vegetative meristems compared to vegetative meristems of TPLATE_3 lines with or
548 without exogenous CLV3 (100 nM) in the growing medium from germination onward. Left panels are merged
549 channels (GFP and PI), right panels are GFP-only channels represented via an intensity scale. Scale bar =
550 20 μ m. The Box plot and jitter box representation graph shows the average fluorescence intensity (8-bit gray
551 values) of CLV1 over the entire SAM (indicated by a dotted line). The box plot extends from the 25th to 75th
552 percentiles. The line inside the box marks the median. The whiskers go down and up to the 95% percentile.
553 Numbers of biological samples from two repeats are indicated at the bottom of the box plot and jitter box
554 graphs. Differences of CLV1-GFP intensity between WDXM2_3 and TPLATE_3 lines under both conditions
555 were evaluated by Welch's ANOVA post hoc pairwise comparison with the Tukey contrasts. Letters (a, b and
556 c) represent significant difference between groups (a,b,c; $P < 0.001$). The quantification is a combination of
557 two independent experiments for each genotype and treatment.



558

559 **Figure 5. TPC interacts with CLV1 through its AtEH1/Pan1 subunit.**

560 (A) Co-immunoprecipitation experiment comparing WT (Col-0) Arabidopsis seedlings and seedlings
 561 expressing pCLV1::CLV1-2xGFP (CLV1) and 35S::eGFP (GFP). CLV1 specifically co-purifies with
 562 endogenous TPLATE. The blue arrow marks full length CLV1 and the magenta arrow marks full length
 563 TPLATE. Numbers next to the ladder represents the protein molecular weight (kDa). The experiment was
 564 independently performed twice with an identical result. (B-C) Representative confocal images and
 565 quantification of ratiometric BiFC analyses exploring the interaction between TPC subunits TPLATE, TML
 566 and AtEH1/Pan1, the AP-2 complex subunit AP2M, and CLV1. The identified interaction between CLV1 and
 567 AtEH1/Pan1 was also performed in the presence of exogenous CLV3 peptide application (1 μ M in infiltration
 568 buffer). CC and NC refer to the orientation of the nYFP and cYFP halves of YFP fused to both proteins. CLV1
 569 was always tagged C-terminally. Left panels in (C) represent the YFP channel, shown via an intensity scale

570 whereas the right panels represent the RFP control channel (free RFP, magenta) against which the intensity
571 of the YFP BiFC channel was normalized. Scale bars = 25 μm . (C) Box plot and jitter box representation
572 showing the quantification of the YFP/RFP fluorescence ratios from two independent experiments. The box
573 plot extends from the 25th to 75th percentiles. The line inside the box marks the median. The whiskers go
574 down and up to the 95% percentile. Numbers of biological samples from at least two independent
575 transformations are indicated at the bottom of the graph. Letters (a, b and c) represent significantly different
576 groups ($P < 0.001$) evaluated by Welch's ANOVA post hoc pairwise comparison with the Tukey contrasts.
577 (D-E) Yeast two hybrid analysis (D) and respective quantification (E) between the cytoplasmic part of CLV1
578 (AA 671-980) and the N-terminal part of AtEH1/Pan1, which ends after the second EH domain (AA 1-527).
579 Combining CLV1 in pGADT7 (AD) with AtEH1/Pan1 in pGBKT7 (BD) allowed growth on selective medium (-
580 L-T-H; strong in 12/24 and weak in 1/24 independent double transformations) whereas only 2/24
581 transformations showed strong and 2/24 showed weak growth on selective medium in the controls, likely
582 caused by some level of auto-activation of AtEH1/Pan1. The negative control consisted of both empty
583 pGBKT7 and pGADT7 vectors (8 independent double transformations) and the positive control (eight
584 independent double transformations) combined pGADT7-SV40 T-Ag with pGBKT7-p53. No: no growth
585 observed on -L-T-H. The data shown represents individual double transformants and the assay was
586 technically repeated twice.

587

588

589

590

591

592

593

594

595

596

597

598

599

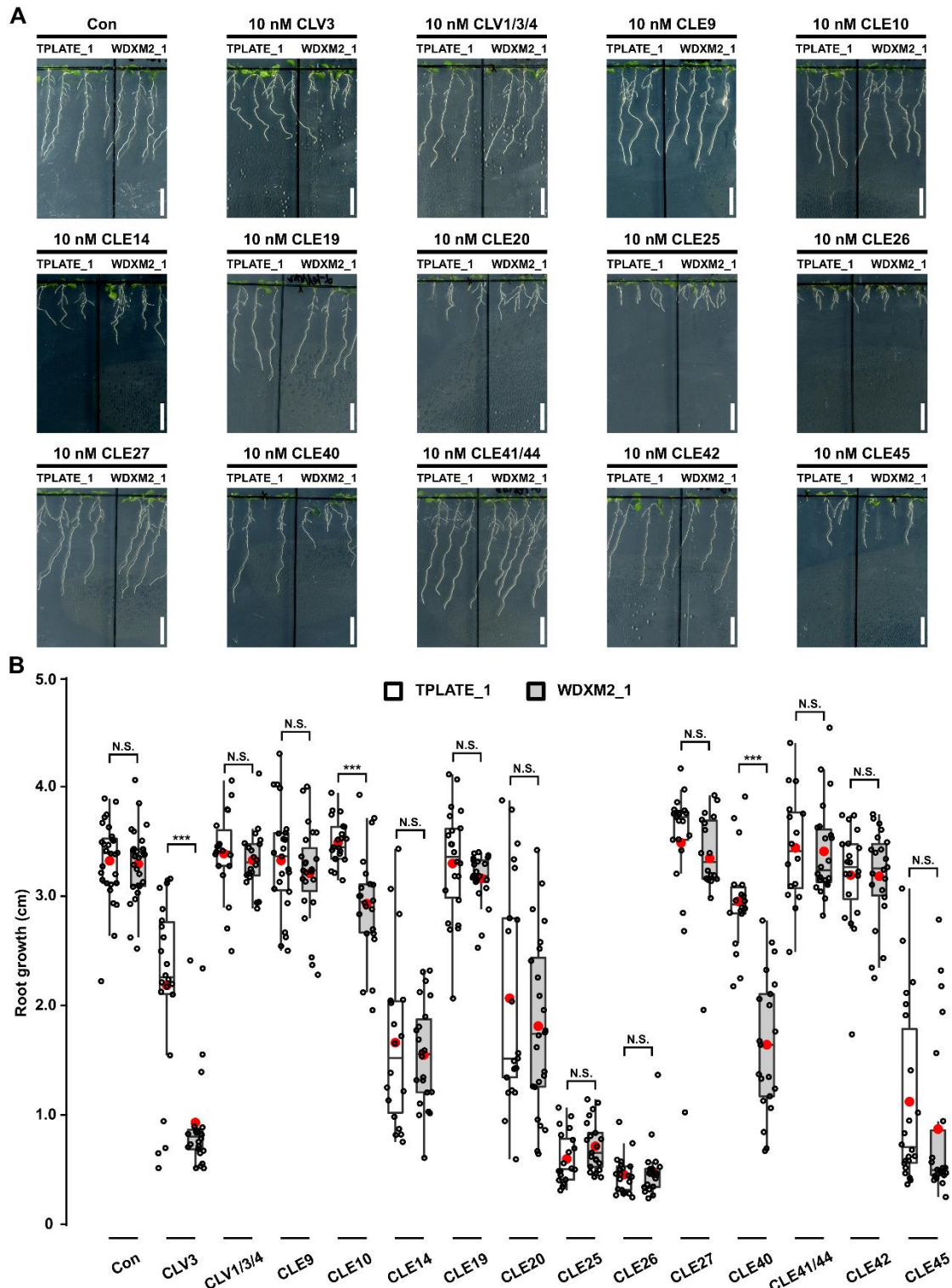
600

601

602

603

604 **Expanded View figures**

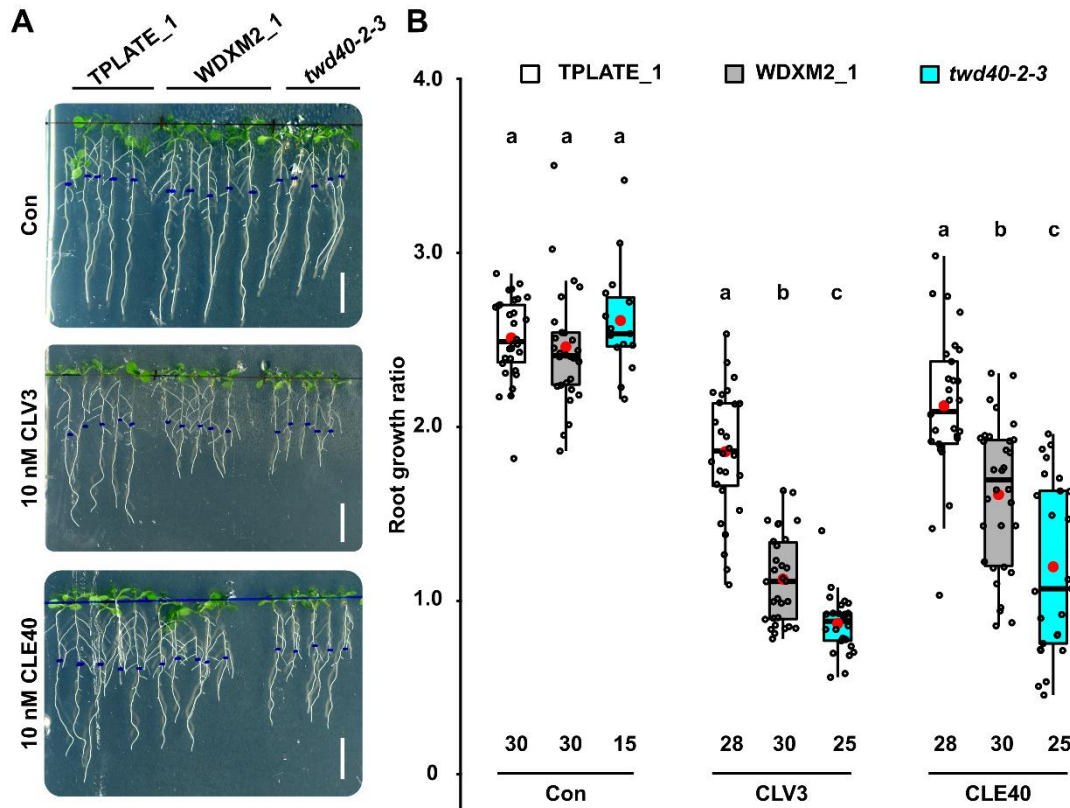


605

606 **Figure EV1. Impaired TPC-dependent endocytic capacity confers hypersensitivity to a subset of CLE**
607 **peptides.**

608 (A-B) Representative images and quantification as box plot and jitter box graphs of the root growth between

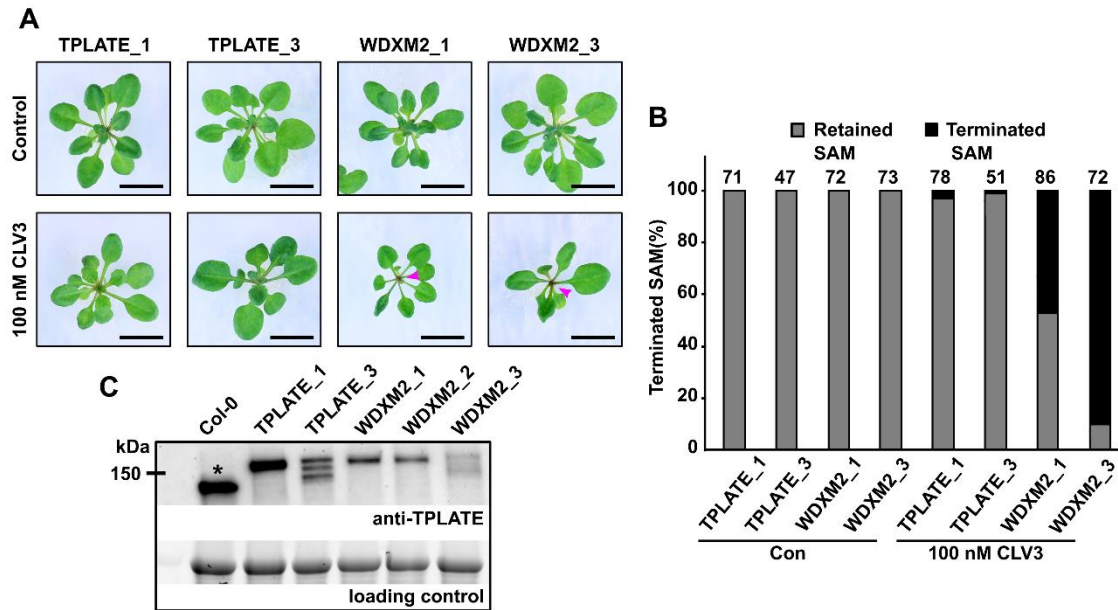
609 TPLATE_1 and WDXM2_1 seedlings grown for 8 days in the presence or absence of low doses (10 nM) of
 610 different CLE peptides. Scale bar = 1cm. Primary root growth was quantified for a number of seedlings (16 ≤
 611 N ≤ 28) and statistically significant differences were observed for CLE10, CLV3 and CLE40. ***, P<0.001
 612 (selected pairs from Welch's ANOVA post hoc pairwise comparison with the Tukey contrasts). N.S., no
 613 significant difference. The experiment was performed twice with a similar outcome. The data represented is
 614 the quantification of one experiment where at least 3 sets of seedlings were grown on separate plates.



615

616 **Figure EV2. The weak TPC subunit mutant allele *twd40-2-3* confirms the observed CLV3 and CLE40**
 617 **hypersensitivity in the WDXM2_1 line.**

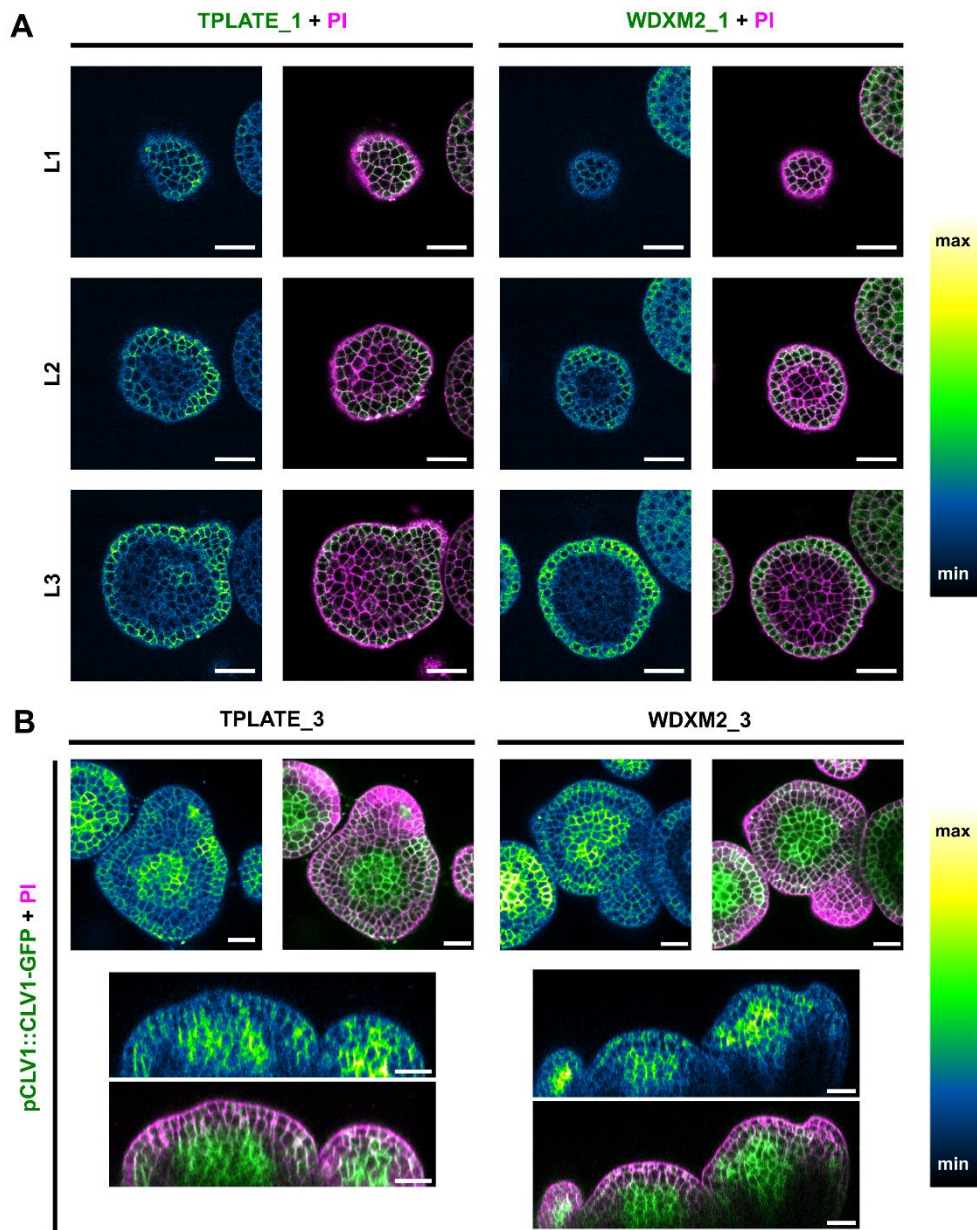
618 (A-B) Representative images (A) and comparison (B) of the primary root growth ratios between TPLATE_1,
 619 WDXM2_1 and *twd40-2-3* seedlings transferred to plates with or without 10 nM CLV3 or CLE40. Root growth
 620 for each root after transfer was divided by the root length before transfer. Numbers of seedlings used for the
 621 quantification are indicated at the bottom of the box plot and jitter box graphs. Scale bar = 1cm. Data
 622 information in panel (B): Differences as compared to TPLATE complemented lines were evaluated by
 623 Welch's ANOVA post hoc pairwise comparison with the Tukey contrasts. Letters (a, b and c) represent
 624 significant difference between groups (P < 0.001). The quantification represented results from at least 5 sets
 625 of seedlings grown on separate plates.



626

627 **Figure EV3. Impaired TPC-dependent endocytic capacity confers CLV3 hypersensitivity in the SAM**
 628 **and this hypersensitivity correlates with the expression level of the complementing construct.**

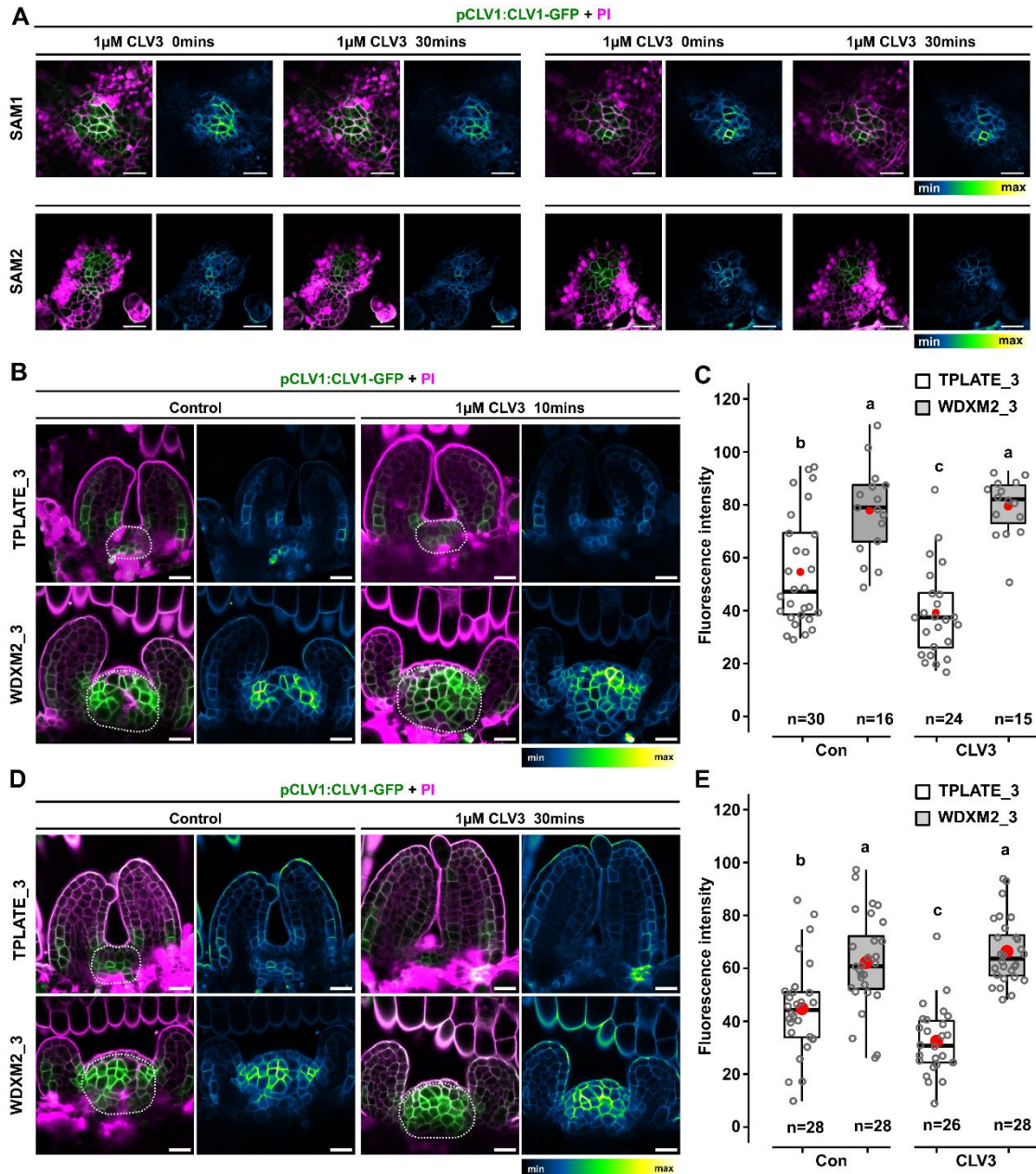
629 (A) Phenotypic comparison of 3 to 4 -week-old independent TPLATE (TPLATE_1 and TPLATE_3) and
 630 WDXM2 (WDXM2_1 and WDXM2_3) lines (GFP and mSCARLET fusions respectively) grown in the
 631 presence or absence of CLV3 peptide. Magenta arrows indicate terminated SAMs. Scale bars = 1 cm. (B)
 632 Quantification of the number of plants with a terminated meristem induced by the CLV3 peptide. The numbers
 633 of plants used for the quantification is indicated at the top of the bar chart. The experiment was repeated
 634 twice and the quantification in panel B combines both experiments. (C) Anti-TPLATE western blot detecting
 635 the presence of endogenous TPLATE in Col-0 (asterisk) as well as the full length of GFP (TPLATE_1,
 636 WDXM2_1 and WDXM2_2) or mSCARLET (TPLATE_3 and WDXM2_3) fusions of TPLATE and WDXM2 in
 637 the complemented *tplate*(*-/-*) homozygous mutant background that lacks endogenous TPLATE. For an
 638 unknown reason, the mSCARLET fusions give rise to several bands on the blot. The WDXM2_2 line showed
 639 a similar expression level as the WDXM2_1 and was not used further. The reduced expression in WDXM2_3
 640 correlates with an increased hypersensitivity to the CLV3 treatment. The large subunit of RUBISCO (around
 641 50 kDa) visualized via the stain free gel, was used as loading control.



642

643 **Figure EV4: TPLATE, WDXM2 and CLV1 expression and localization in flower meristems.**

644 (A) Serial optical cross sections through the inflorescence meristem, showing localization of TPLATE and
645 WDXM2 in layer 1 to 3 (L1-L2-L3). Left images are intensity scaled. Images on the right for each genotype
646 represent the merged GFP and PI channels. Scale bar = 25 μ m. (B) Representative confocal images showing
647 the localization of CLV1-GFP in inflorescence meristems of TPLATE_3 and WDXM2_3 lines in optical cross
648 sections (upper panel), and orthogonal views (lower panel). Scale bar = 20 μ m.



649

650 **Figure EV5. Reduced TPC-dependent endocytic capacity impairs internalization of CLV1 from PM in**
 651 **vegetative SAM cells upon short-term CLV3 treatment.**

652 (A) Representative images of two vegetative SAMs in the TPLATE_3 background, with different levels of
 653 CLV1 expression, imaged before and after exogenous CLV3 treatment (1 μ M for 30 min). Two different focal
 654 planes of a Z-stack, visualizing different L3 cells per SAM are represented for each timepoint. For both SAMs,
 655 the CLV1 intensity at PM reduces upon CLV3 treatment. (B-E) Representative confocal images and
 656 quantification of Arabidopsis TPLATE_3 and WDXM2_3 expressing seedlings following short-term CLV3
 657 peptide treatment (1 μ M for 10 min: B-C and 1 μ M for 30 min: D-E). Similar to the long-term treatment (Fig
 658 4), PM localization of CLV1-GFP reduces upon CLV3 peptide treatment, which is not the case in WDXM2_3
 659 vegetative meristems. The box plot and jitter box representation graph represents the average fluorescence
 660 intensity (8-bit gray values) of CLV1 over the entire SAM (indicated by a dotted line). Numbers of biological

26

661 samples from two repeats are indicated at the bottom of the box plot and jitter box graphs. Differences of
 662 CLV1-GFP intensity between WDXM2_3 and TPLATE_3 lines under both conditions were evaluated by
 663 Welch's ANOVA post hoc pairwise comparison with the Tukey contrasts. Letters (a, b and c) represent
 664 significant difference between groups (a and b, $P < 0.001$; b and c, $P < 0.05$). The quantification combines
 665 at least two independent experiments for each genotype, treatment and duration of treatment. Left panels
 666 are merged channels (GFP and PI), right panels are GFP-only channels represented via an intensity scale.
 667 Scale bar = 20 μm .

668 Expanded View tables

669 Table EV1: list of used Arabidopsis lines

670 The table provides an overview of the lines used, their genetic background and
 671 references. H: Hygromycin; B: Basta; GPCR: Genotyping PCR; (-/-): homozygous mutant
 672 background; (+/-): heterozygous mutant background.

Plant lines	Full name	Background	Antibiotic selection	Identification	Resources
<i>tplate</i>		(+/-) (+/+)		GPCR	Van Damme et al., 2006
<i>twd40-2-3</i>		(-/-)		GPCR	Bashline et al., 2015
TPLATE_1	pLAT52-TPLATE-GFP	<i>tplate</i> (-/-)	H	GPCR	Van Damme et al., 2006
TPLATE_3	pLAT52-TPLATE-mScarlet	<i>tplate</i> (-/-)	H	GPCR	This study
WDXM2_1	pLAT52-WDXM2-GFP	<i>tplate</i> (-/-)	B	GPCR	Wang et al., 2021
WDXM2_2	pLAT52-WDXM2-GFP	<i>tplate</i> (-/-)	B	GPCR	Wang et al., 2021
WDXM2_3	pLAT52-WDXM2-mScarlet	<i>tplate</i> (-/-)	H	GPCR	This study
<i>clv1-101</i>		(-/-)			Kinoshita et al, 2010
<i>clv1-8</i>		(-/-)			Dievart et al., 2003
TPLATE_1 <i>clv1-101</i>	pLAT52-TPLATE-GFP	<i>tplate</i> (-/-) <i>clv1-101</i> (-/-)		GPCR	This study
WDXM2_1 <i>clv1-101</i>	pLAT52-WDXM2-GFP	<i>tplate</i> (-/-) <i>clv1-101</i> (-/-)		GPCR	This study
TPLATE_1 <i>clv1-8</i>	pLAT52-TPLATE-GFP	<i>tplate</i> (-/-) <i>clv1-8</i> (-/-)		GPCR, Sequence	This study
WDXM2_1 <i>clv1-8</i>	pLAT52-WDXM2-GFP	<i>tplate</i> (-/-) <i>clv1-8</i> (-/-)		GPCR, Sequence	This study
WUS-GUS	pWUS-GUS	<i>Col_0</i>			Su et al., 2009

TPLATE_1 pWUS-GUS	pLAT52-TPLATE-GFP/pWUS-GUS	<i>tplate (-/-)</i>		GPCR, GUS staining	This study
WDXM2_1 pWUS-GUS	pLAT52-WDXM2-GFP/pWUS-GUS	<i>tplate (-/-)</i>		GPCR, GUS staining	This study
CLV1-GFP	pCLV1-CLV1-GFP	<i>Col_0</i>			Prof. Rüdiger Simon
TPLATE_3 CLV1-GFP	pLAT52-TPLATE-mScarlet/pCLV1-CLV1-GFP	<i>tplate (-/-)</i>		GPCR, Basta	This study
WDXM2_3 CLV1-GFP	pLAT52-WDXM2-mScarlet/pCLV1-CLV1-GFP	<i>tplate (-/-)</i>		GPCR, Basta	This study
eGFP	p35S-eGFP	<i>Col-0</i>			Obtained from Prof. E. Russinova

673

674 **Table EV2: Information of CLE peptides used in this research.**

675 The table provides an overview of the sequences of the various CLE peptides used, their
676 molecular weight (MW), purify and stock concentration. Hyp: Hydroxyproline; Ara:
677 Arabinosylated.

	Name	Sequence and modifications	MW	Purity (%)	Stock solution
1	CLV3	RTVHypSG[Ara3]HypDPLHHH	1449,58	95,7	100 µM/water
2	CLE1/3/4	RLSPGGPDPRHH	1325,44	94,3	100 µM/water
3	CLE9	RLVHypSGHypNPLHN+[Ara3], [Ara4] or[Ara6]	1300,47	95	100 µM/water
4	CLE10	RLVPSGPNPLHN	1300,47	98,4	100 µM/water
5	CLE14	RLVPKGNPLHN	1341,57	84,8	100 µM/water
6	CLE19	RVIPTGPNPLHN	1314,5	85,6	100 µM/water
7	CLE20	RKVKTGSNPLHN	1350,53	96,5	100 µM/water
8	CLE25	RKVPNGPDIHN	1340,5	94,4	100 µM/water
9	CLE26	RKVPRGPDPIHN	1385,58	91,2	100 µM/water
10	CLE27	RIVPSCPDPLHN	1347,55	74,2	100 µM/water
11	CLE40	RQVPTGSDPLHH	1343,45	92,5	100 µM/water
12	CLE41/44	HEVPSGPNPISN	1247,32	89,9	100 µM/water
13	CLE42	HGVPSGPNPISN	1175,26	93,9	100 µM/water
14	CLE45	RRVRRGSDPIHN	1462,63	88,6	100 µM/water

678

679

680 **Acknowledgements**

681 We would like to thank Elliot Meyerowitz, Marcus Heisler and Thomas Laux for
682 constructive discussions. This work was supported by the European Research Council,
683 Grant 682436 to D.V.D.; the Research Foundation–Flanders, Grant 1226420N to P.G.;
684 The China Scholarship Council, grant 201508440249 to J.W.; grant 201906760018 to
685 Q.J. and grant 201706350153 to X.X.; and by Ghent University Special Research co-
686 funding, grant ST01511051 to J.W.

687 **Author contributions**

688 J.W., Q.J., R.P. and P.G. designed and performed experiments. G.D. provided
689 unpublished materials. C.G-A. and E. B. designed and performed floral SAM imaging.
690 E.B performed vegetative SAM Z-stack vertical imaging. X.X. and P.G. performed co-IP.
691 M.V. performed Y2H. E.M. performed confocal imaging. R.P., I.D.S., T.V., R.S., M. K. N.
692 and D.V.D. designed and supervised research. J.W., R.P., and D.V.D wrote the initial
693 draft of the manuscript. All authors were involved in discussing the data and in finalizing
694 the conclusions and text of the manuscript.

695 **Disclosure and competing interests statements**

696 The authors declare that they have no conflict of interest.

697 **Data availability**

698 This study includes no data deposited in external repositories. Data used for
699 quantifications as well as full Western blots can be found in the source data file. All
700 material will be made available upon reasonable request to the corresponding author
701 (daniel.vandamme@psb.vib-ugent.be).

702 **References**

703 Anne P, Amiguet-Vercher A, Brandt B, Kalmbach L, Geldner N, Hothorn M, Hardtke CS (2018)
704 CLERK is a novel receptor kinase required for sensing of root-active CLE peptides in Arabidopsis.
705 *Development* 145
706 Arora D, Abel NB, Liu C, Van Damme P, Yperman K, Eeckhout D, Vu LD, Wang J, Tornkvist A,
707 Impens F *et al* (2020) Establishment of Proximity-Dependent Biotinylation Approaches in Different
708 Plant Model Systems. *Plant Cell* 32: 3388-3407
709 Arora D, Damme DV (2021) Motif-based endomembrane trafficking. *Plant Physiol* 186: 221-238
710 Atsuko Kinoshita SB, Yuriko Osakabe, Shinji Mizuno, Shingo Nagawa, Yvonne Stahl, Rüdiger
711 Simon, Kazuko Yamaguchi-Shinozaki, Hiroo Fukuda and Shinichiro Sawa (2010) RPK2 is an
712 essential receptor-like kinase that transmits the CLV3 signal in Arabidopsis. *Development*
713 Bashline L, Li S, Zhu X, Gu Y (2015) The TWD40-2 protein and the AP2 complex cooperate in the
714 clathrin-mediated endocytosis of cellulose synthase to regulate cellulose biosynthesis. *Proc Natl*
715 *Acad Sci U S A* 112: 12870-12875

- 716 Beck M, Zhou J, Faulkner C, MacLean D, Robatzek S (2012) Spatio-temporal cellular dynamics
717 of the Arabidopsis flagellin receptor reveal activation status-dependent endosomal sorting. *Plant*
718 *Cell* 24: 4205-4219
- 719 Ben Khaled S, Postma J, Robatzek S (2015) A moving view: subcellular trafficking processes in
720 pattern recognition receptor-triggered plant immunity. *Annu Rev Phytopathol* 53: 379-402
- 721 Bindels DS, Haarbosch L, van Weeren L, Postma M, Wiese KE, Mastop M, Aumonier S, Gotthard
722 G, Royant A, Hink MA *et al* (2017) mScarlet: a bright monomeric red fluorescent protein for cellular
723 imaging. *Nat Methods* 14: 53-56
- 724 Blumke P, Schlegel J, Gonzalez-Ferrer C, Becher S, Pinto KG, Monaghan J, Simon R (2021)
725 Receptor-like cytoplasmic kinase MAZZA mediates developmental processes with CLAVATA1
726 family receptors in Arabidopsis. *J Exp Bot* 72: 4853-4870
- 727 Brand U, Fletcher JC, Hobe M, Meyerowitz EM, Simon R (2000) Dependence of stem cell fate in
728 Arabidopsis on a feedback loop regulated by CLV3 activity. *Science* 289: 617-619
- 729 Breda AS, Hazak O, Schultz P, Anne P, Graeff M, Simon R, Hardtke CS (2019) A Cellular Insulator
730 against CLE45 Peptide Signaling. *Curr Biol* 29: 2501-2508 e2503
- 731 Brunoud G, Galvan-Ampudia CS, Vernoux T (2020) Methods to Visualize Auxin and Cytokinin
732 Signaling Activity in the Shoot Apical Meristem. *Methods Mol Biol* 2094: 79-89
- 733 Clark SE, Running MP, Meyerowitz EM (1993) CLAVATA1, a regulator of meristem and flower
734 development in Arabidopsis. *Development* 119: 397-418
- 735 Clark SE, Running MP, Meyerowitz EM (1995) Clavata3 Is a Specific Regulator of Shoot and
736 Floral Meristem Development Affecting the Same Processes as Clavata1. *Development* 121:
737 2057-2067
- 738 Clark SE, Williams RW, Meyerowitz EM (1997) The CLAVATA1 Gene Encodes a Putative
739 Receptor Kinase That Controls Shoot and Floral Meristem Size in Arabidopsis. *Cell* 89: 575-585
- 740 Claus LAN, Savatin DV, Russinova E (2018) The crossroads of receptor-mediated signaling and
741 endocytosis in plants. *J Integr Plant Biol* 60: 827-840
- 742 Dejonghe W, Kuenen S, Mylle E, Vasileva M, Keech O, Viotti C, Swerts J, Fendrych M, Ortiz-
743 Morea FA, Mishev K *et al* (2016) Mitochondrial uncouplers inhibit clathrin-mediated endocytosis
744 largely through cytoplasmic acidification. *Nat Commun* 7: 11710
- 745 Dejonghe W, Sharma I, Denoo B, De Munck S, Lu Q, Mishev K, Bulut H, Mylle E, De Rycke R,
746 Vasileva M *et al* (2019) Disruption of endocytosis through chemical inhibition of clathrin heavy
747 chain function. *Nat Chem Biol* 15: 641-649
- 748 DeYoung BJ, Bickle KL, Schrage KJ, Muskett P, Patel K, Clark SE (2006) The CLAVATA1-related
749 BAM1, BAM2 and BAM3 receptor kinase-like proteins are required for meristem function in
750 Arabidopsis. *Plant J* 45: 1-16
- 751 DeYoung BJ, Clark SE (2008) BAM receptors regulate stem cell specification and organ
752 development through complex interactions with CLAVATA signaling. *Genetics* 180: 895-904
- 753 Di Rubbo S, Irani NG, Kim SY, Xu ZY, Gadeyne A, Dejonghe W, Vanhoutte I, Persiau G, Eeckhout
754 D, Simon S *et al* (2013) The clathrin adaptor complex AP-2 mediates endocytosis of
755 brassinosteroid insensitive1 in Arabidopsis. *Plant Cell* 25: 2986-2997
- 756 Dievart A, Dalal M, Tax FE, Lacey AD, Huttly A, Li J, Clark SE (2003) CLAVATA1 dominant-
757 negative alleles reveal functional overlap between multiple receptor kinases that regulate
758 meristem and organ development. *Plant Cell* 15: 1198-1211
- 759 Fletcher JC, Brand U, Running MP, Simon R, Meyerowitz EM (1999) Signaling of cell fate
760 decisions by CLAVATA3 in Arabidopsis shoot meristems. *Science* 283: 1911-1914
- 761 Gadeyne A, Sanchez-Rodriguez C, Vanneste S, Di Rubbo S, Zauber H, Vanneste K, Van Leene
762 J, De Winne N, Eeckhout D, Persiau G *et al* (2014) The TPLATE adaptor complex drives clathrin-
763 mediated endocytosis in plants. *Cell* 156: 691-704
- 764 Gou X, Li J (2020) Paired Receptor and Coreceptor Kinases Perceive Extracellular Signals to
765 Control Plant Development. *Plant Physiol* 182: 1667-1681
- 766 Graeff M, Rana S, Marhava P, Moret B, Hardtke CS (2020) Local and Systemic Effects of
767 Brassinosteroid Perception in Developing Phloem. *Curr Biol* 30: 1626-1638 e1623
- 768 Grefen C, Blatt MR (2012) A 2in1 cloning system enables ratiometric bimolecular fluorescence
769 complementation (rBiFC). *Biotechniques* 53: 311-314
- 770 Hazak O, Brandt B, Cattaneo P, Santiago J, Rodriguez-Villalon A, Hothorn M, Hardtke CS (2017)
771 Perception of root-active CLE peptides requires CORYNE function in the phloem vasculature.
772 *EMBO Rep* 18: 1367-1381
- 773 Hazak O, Hardtke CS (2016) CLAVATA 1-type receptors in plant development. *J Exp Bot* 67:
774 4827-4833

- 775 Herberich E, Sikorski J, Hothorn T (2010) A robust procedure for comparing multiple means under
776 heteroscedasticity in unbalanced designs. *PLoS ONE* 5: e9788
- 777 Hirst J, Schlacht A, Norcott JP, Traynor D, Bloomfield G, Antrobus R, Kay RR, Dacks JB, Robinson
778 MS (2014) Characterization of TSET, an ancient and widespread membrane trafficking complex.
779 *eLife* 3: e02866
- 780 Hobe M, Muller R, Grunewald M, Brand U, Simon R (2003) Loss of CLE40, a protein functionally
781 equivalent to the stem cell restricting signal CLV3, enhances root waving in Arabidopsis. *Dev*
782 *Genes Evol* 213: 371-381
- 783 Hohmann U, Lau K, Hothorn M (2017) The Structural Basis of Ligand Perception and Signal
784 Activation by Receptor Kinases. *Annu Rev Plant Biol* 68: 109-137
- 785 Hu C, Zhu Y, Cui Y, Cheng K, Liang W, Wei Z, Zhu M, Yin H, Zeng L, Xiao Y *et al* (2018) A group
786 of receptor kinases are essential for CLAVATA signalling to maintain stem cell homeostasis. *Nat*
787 *Plants* 4: 205-211
- 788 Irani NG, Di Rubbo S, Mylle E, Van den Begin J, Schneider-Pizon J, Hnilikova J, Sisa M, Buyst D,
789 Vilarrasa-Blasi J, Szatmari AM *et al* (2012) Fluorescent castasterone reveals BR11 signaling from
790 the plasma membrane. *Nat Chem Biol* 8: 583-589
- 791 Ishida T, Tabata R, Yamada M, Aida M, Mitsumasu K, Fujiwara M, Yamaguchi K, Shigenobu S,
792 Higuchi M, Tsuji H *et al* (2014) Heterotrimeric G proteins control stem cell proliferation through
793 CLAVATA signaling in Arabidopsis. *EMBO Rep* 15: 1202-1209
- 794 Ito Y, Nakanomyo I, Motose H, Iwamoto K, Sawa S, Dohmae N, Fukuda H (2006) Dodeca-CLE
795 peptides as suppressors of plant stem cell differentiation. *Science* 313: 842-845
- 796 Johnson A, Dahhan DA, Gnyliukh N, Kaufmann WA, Zheden V, Costanzo T, Mahou P, Hryan M,
797 Wang J, Aguilera-Servin J *et al* (2021) The TPLATE complex mediates membrane bending during
798 plant clathrin-mediated endocytosis. *Proc Natl Acad Sci U S A* 118
- 799 Karimi M, Depicker A, Hilson P (2007) Recombinational cloning with plant gateway vectors. *Plant*
800 *Physiol* 145: 1144-1154
- 801 Kitagawa M, Jackson D (2019) Control of Meristem Size. *Annu Rev Plant Biol* 70: 269-291
- 802 Lammens T, Boudolf V, Kheibarshekan L, Zalmas LP, Gaamouche T, Maes S, Vanstraelen M,
803 Kondorosi E, La Thangue NB, Govaerts W *et al* (2008) Atypical E2F activity restrains
804 APC/CCCS52A2 function obligatory for endocycle onset. *Proc Natl Acad Sci U S A* 105: 14721-
805 14726
- 806 Liu D, Kumar R, Claus LAN, Johnson AJ, Siao W, Vanhoutte I, Wang P, Bender KW, Yperman K,
807 Martins S *et al* (2020) Endocytosis of BRASSINOSTEROID INSENSITIVE1 Is Partly Driven by a
808 Canonical Tyr-Based Motif. *Plant Cell* 32: 3598-3612
- 809 Mbengue M BG, Gervasi F, Beck M, Zhou J, Spallek T, Bartels S, Boller T, Ueda T, Kuhn H,
810 Robatzek S (2016) Clathrin-dependent endocytosis is required for immunity mediated by pattern
811 recognition receptor kinases. *Proc Natl Acad Sci USA* 113: 11034-11039
- 812 Meijering E, Jacob M, Sarria JC, Steiner P, Hirling H, Unser M (2004) Design and validation of a
813 tool for neurite tracing and analysis in fluorescence microscopy images. *Cytometry A* 58: 167-176
- 814 Mishev K, Lu Q, Denoo B, Peurois F, Dejonghe W, Hullaert J, De Rycke R, Boeren S, Bretou M,
815 De Munck S *et al* (2018) Nonselective Chemical Inhibition of Sec7 Domain-Containing ARF
816 GTPase Exchange Factors. *Plant Cell* 30: 2573-2593
- 817 Nimchuk ZL (2017) CLAVATA1 controls distinct signaling outputs that buffer shoot stem cell
818 proliferation through a two-step transcriptional compensation loop. *PLoS Genet* 13: e1006681
- 819 Nimchuk ZL, Tarr PT, Ohno C, Qu X, Meyerowitz EM (2011) Plant stem cell signaling involves
820 ligand-dependent trafficking of the CLAVATA1 receptor kinase. *Curr Biol* 21: 345-352
- 821 Nimchuk ZL, Zhou Y, Tarr PT, Peterson BA, Meyerowitz EM (2015) Plant stem cell maintenance
822 by transcriptional cross-regulation of related receptor kinases. *Development* 142: 1043-1049
- 823 Ogawa M, Shinohara H, Sakagami Y, Matsubayashi Y (2008) Arabidopsis CLV3 peptide directly
824 binds CLV1 ectodomain. *Science* 319: 294
- 825 Olsson V, Joos L, Zhu S, Gevaert K, Butenko MA, De Smet I (2019) Look Closely, the Beautiful
826 May Be Small: Precursor-Derived Peptides in Plants. *Annu Rev Plant Biol* 70: 153-186
- 827 Ortiz-Morea FA, Savatin DV, Dejonghe W, Kumar R, Luo Y, Adamowski M, Van den Begin J,
828 Dressano K, Pereira de Oliveira G, Zhao X *et al* (2016) Danger-associated peptide signaling in
829 Arabidopsis requires clathrin. *Proc Natl Acad Sci U S A* 113: 11028-11033
- 830 Paez Valencia J, Goodman K, Otegui MS (2016) Endocytosis and Endosomal Trafficking in Plants.
831 *Annu Rev Plant Biol* 67: 309-335
- 832 Poncini L, Wyrsh I, Denervaud Tendon V, Vorley T, Boller T, Geldner N, Metraux JP, Lehmann
833 S (2017) In roots of Arabidopsis thaliana, the damage-associated molecular pattern AtPep1 is a

834 stronger elicitor of immune signalling than flg22 or the chitin heptamer. *PLoS ONE* 12: e0185808
835 Roberts I, Smith S, Stes E, De Rybel B, Staes A, van de Cotte B, Njo MF, Dedeyne L, Demol H,
836 Lavenus J *et al* (2016) CEP5 and XIP1/CEPR1 regulate lateral root initiation in Arabidopsis. *J Exp*
837 *Bot* 67: 4889-4899
838 Schlegel J, Denay G, Wink R, Pinto KG, Stahl Y, Schmid J, Blumke P, Simon RG (2021) Control
839 of Arabidopsis shoot stem cell homeostasis by two antagonistic CLE peptide signalling pathways.
840 *eLife* 10
841 Schoof H, Lenhard M, Haecker A, Mayer KFX, Jürgens G, Laux T (2000) The Stem Cell Population
842 of Arabidopsis Shoot Meristems Is Maintained by a Regulatory Loop between the CLAVATA and
843 WUSCHEL Genes. *Cell* 100: 635-644
844 Shinohara H, Matsubayashi Y (2015) Reevaluation of the CLV3-receptor interaction in the shoot
845 apical meristem: dissection of the CLV3 signaling pathway from a direct ligand-binding point of
846 view. *Plant J* 82: 328-336
847 Somssich M, Ma Q, Weidtkamp-Peters S, Stahl Y, Felekyan S, Bleckmann A, Seidel CA, Simon
848 R (2015) Real-time dynamics of peptide ligand-dependent receptor complex formation in planta.
849 *Sci Signal* 8: ra76
850 Stahl Y, Grabowski S, Bleckmann A, Kuhnemuth R, Weidtkamp-Peters S, Pinto KG, Kirschner
851 GK, Schmid JB, Wink RH, Hulsewede A *et al* (2013) Moderation of Arabidopsis root stemness by
852 CLAVATA1 and ARABIDOPSIS CRINKLY4 receptor kinase complexes. *Curr Biol* 23: 362-371
853 Stahl Y, Wink RH, Ingram GC, Simon R (2009) A signaling module controlling the stem cell niche
854 in Arabidopsis root meristems. *Curr Biol* 19: 909-914
855 Su YH, Zhao XY, Liu YB, Zhang CL, O'Neill SD, Zhang XS (2009) Auxin-induced WUS expression
856 is essential for embryonic stem cell renewal during somatic embryogenesis in Arabidopsis. *Plant*
857 *J* 59: 448-460
858 Van Damme D, Coutuer S, De Rycke R, Bouget FY, Inze D, Geelen D (2006) Somatic cytokinesis
859 and pollen maturation in Arabidopsis depend on TPLATE, which has domains similar to coat
860 proteins. *Plant Cell* 18: 3502-3518
861 Van Leene J, Eeckhout D, Cannoot B, De Winne N, Persiau G, Van De Slijke E, Vercruyse L,
862 Dedecker M, Verkest A, Vandepoele K *et al* (2015) An improved toolbox to unravel the plant
863 cellular machinery by tandem affinity purification of Arabidopsis protein complexes. *Nat Protoc* 10:
864 169-187
865 Wang J, Mylle E, Johnson A, Besbrugge N, De Jaeger G, Friml J, Pleskot R, Van Damme D (2020)
866 High Temporal Resolution Reveals Simultaneous Plasma Membrane Recruitment of TPLATE
867 Complex Subunits. *Plant Physiol* 183: 986-997
868 Wang J, Yperman K, Gronos P, Jiang Q, Dragwidge J, Mylle E, Mor E, Nolf J, Eeckhout D, De
869 Jaeger G *et al* (2021) Conditional destabilization of the TPLATE complex impairs endocytic
870 internalization. *Proc Natl Acad Sci U S A* 118
871 Wang P, Pleskot R, Zang J, Winkler J, Wang J, Yperman K, Zhang T, Wang K, Gong J, Guan Y
872 *et al* (2019) Plant AtEH/Pan1 proteins drive autophagosome formation at ER-PM contact sites
873 with actin and endocytic machinery. *Nat Commun* 10: 5132
874 Yamaguchi YL, Ishida T, Sawa S (2016) CLE peptides and their signaling pathways in plant
875 development. *J Exp Bot* 67: 4813-4826
876 Yperman K, Papageorgiou AC, Merceron R, De Munck S, Bloch Y, Eeckhout D, Jiang Q, Tack P,
877 Grigoryan R, Evangelidis T *et al* (2021a) Distinct EH domains of the endocytic TPLATE complex
878 confer lipid and protein binding. *Nat Commun* 12: 3050
879 Yperman K, Wang J, Eeckhout D, Winkler J, Vu LD, Vandorpe M, Gronos P, Mylle E, Kraus M,
880 Merceron R *et al* (2021b) Molecular architecture of the endocytic TPLATE complex. *Sci Adv* 7
881 Zhang Y, Persson S, Hirst J, Robinson MS, van Damme D, Sanchez-Rodriguez C (2015) Change
882 your TPLATE, change your fate: plant CME and beyond. *Trends Plant Sci* 20: 41-48

883